Use of fura red as an intracellular calcium indicator in frog skeletal muscle fibers

Nagomi Kurebayashi, A. B. Harkins, and S. M. Baylor
Department of Physiology, University of Pennsylvania School of Medicine, Philadelphia, Pennsylvania 19104-6085 USA

ABSTRACT Fura red, a fluorescent Ca^{2+} indicator with absorbance bands at visible wavelengths, was injected into intact single muscle fibers that had been stretched to a long sarcomere length (~3.8 μm) and bathed in a 'high-Ca^{2+}' Ringer ($[Ca^{2+}]$ = 11.8 mM). From fura red's slow diffusion coefficient in myoplasm, 0.16 (±0.01, SEM) × 10^{-6} cm^2 s^{-1} (N = 5; 16°C), it is estimated that ~85% of the indicator molecules are bound to muscle constituents of large molecular weight. Binding appears to elevate, by 3- to 4-fold, the indicator's apparent dissociation constant for Ca^{2+} (K_D), which is estimated to be 1.1–1.6 μM in myoplasm. Fura red's myoplasmic absorbance spectrum was used to estimate f_r, the fraction of fura red molecules in the Ca^{2+}-bound form at rest. In 3 fibers thought to be minimally damaged by the micro-injection, f_r was estimated to be 0.15 (±0.01). Thus, resting myoplasmic free $[Ca^{2+}]$ ($[Ca^{2+}]_r$) is estimated to be 0.19–0.28 μM. For fibers in normal Ringer solution ($[Ca^{2+}]$ = 1.8 mM), at shorter sarcomere length (~2.7 μm), and containing a nonperturbing concentration of indicator (≤0.2 mM), $[Ca^{2+}]_r$ is estimated to be 0.18–0.27 μM. This range is higher than estimated previously in frog fibers with other techniques.

In 6 fibers, R, the indicator's fluorescence ratio signal (equal to the emission intensity measured with 420 nm excitation divided by that measured with 480 nm excitation), was measured at rest and following electrical stimulation and compared with absorbance measurements made from the same fiber region. The analysis implies that R_{MIN} and R_{MAX} (the values of R that would be measured if all indicator molecules were in the Ca^{2+}-free and Ca^{2+}-bound states, respectively) were substantially smaller in myoplasm than in calibration solutions lacking muscle proteins. Several methods for estimation of $[Ca^{2+}]_r$ from R are analyzed and discussed.

INTRODUCTION

A large body of experimental work concerns the measurement of cytoplasmic free $[Ca^{2+}]$, both in quiescent cells and in cells responding to external stimuli. In recent years, this work has been greatly aided by the availability of Ca^{2+} indicator molecules from the "tetracarboxylate" family of compounds (1), such as quin-2 (2), indo-1 and fura-2 (3), and fluo-3 (4). Upon complexation with Ca^{2+}, these indicators undergo a large change in absorbance and/or fluorescence; furthermore, they react with Ca^{2+} with high-affinity, simple stoichiometry (1 Ca^{2+} to 1 indicator molecule), and with little interference from potentially competing ions such as Mg^{2+} and protons.

Amphibian skeletal muscle fibers represent a cell type where $[Ca^{2+}]$ has been studied extensively, not only with tetracarboxylate indicators (5–10), but with other methods as well, including aequorin (11–15); Ca^{2+}-selective micro-electrodes (15–18); absorbance indicators such as arsenazo III (19–23), antipyrylazo III (22–26) and members of the purpurate family of Ca^{2+} indicators (27–29); and furaptra (30), a "tricarboxylate" fluorescence indicator (31).

Unfortunately, many of the above studies have reported methodological difficulties that render uncertain quantitative information about $[Ca^{2+}]$. For example, both aequorin and all of the above-mentioned indicator dyes appear to bind to intracellular constituents such as soluble and/or structural proteins. In most cases this binding appears to alter significantly the calibration of the Ca^{2+} signal from the indicator (see, for example, references 26, 32, 15). Moreover, with intact (as opposed to cut) skeletal muscle fibers, all of the above techniques require micro-electrode impalements, which, without care, can elevate myoplasmic $[Ca^{2+}]$ (15). Thus, uncertainty exists concerning the accuracy of the information obtained, for both resting $[Ca^{2+}]$ ($[Ca^{2+}]_r$) and the changes in $[Ca^{2+}]$ ($\Delta[Ca^{2+}]$) that occur in response to electrical stimulation.

In the studies that corrected for the effect of the intracellular environment on the indicator's calibration of $[Ca^{2+}]$, the following estimates were obtained: (a) for the peak of $\Delta[Ca^{2+}]$ triggered by a single action potential, 20–30 μM in cut fibers (26–28) and 10–15 μM in intact fibers (29–30); (b) for $[Ca^{2+}]_r$, ~50 nM in cut fibers (6) and less than 60 nM in intact fibers (15). The latter study (15) reported an upper limit only, because the methodologies employed, aequorin and Ca^{2+}-selective micro-electrodes, were not sufficiently sensitive to reliably detect $[Ca^{2+}]_r$ at the normal resting level.

In this paper we describe the use of fura red, a new high-affinity Ca^{2+} indicator dye (33), to study $[Ca^{2+}]_r$ in frog muscle. Fura red is chemically similar to fura-2 (Fig. 1), but, in contrast to fura-2, has major absorbance and fluorescence-excitation bands at visible rather than ultra-violet wavelengths. Thus, absorbance measurements with fura red should be more accurate than with fura-2 because interference from the intrinsic absorbance of the fiber is substantially smaller at visible wavelengths (34, 35).

Address correspondence to Dr. S. M. Baylor, Department of Physiology, University of Pennsylvania School of Medicine, Philadelphia, PA 19104-6085.

Current address of Dr. Kurebayashi is the Department of Pharmacology, Juntendo University School of Medicine, 2-1-1 Hongo, Bunkyo-ku, Tokyo 113, Japan.

0006-3495/93/06/1934/27 $2.00

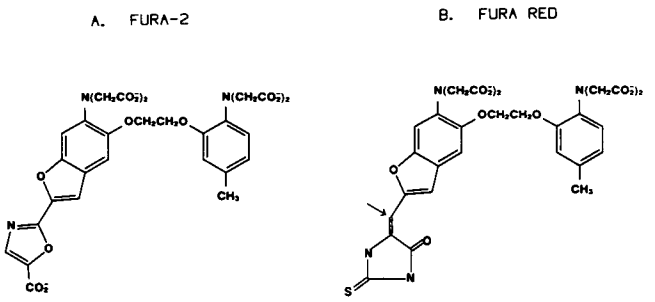

FIGURE 1 (*A*) Structure of pentavalent fura-2; molecular weight, 637 (from ref. 3). (*B*) Structure of tetravalent fura red; molecular weight, 652 (from the 1992 catalogue of Molecular Probes, Inc). A photo-isomerization of fura red may occur about the carbon atom pointed to by the arrow (personal communication of Dr. Richard P. Haugland of Molecular Probes, Inc.).

This article reaches three principal conclusions from the measurements with fura red. First, with single fibers that contain ≥0.2–0.3 mM indicator, resting absorbance measurements permit estimation of the fraction of the indicator in the Ca^{2+}-bound form at rest. Second, simultaneous measurements of the indicator's absorbance and fluorescence signals in a fiber permit construction of an "in-situ" calibration of the indicator's fluorescence ratio signal under physiological conditions. Interestingly, this in-situ calibration is substantially different from that measured from the indicator under in vitro conditions in 0.1 M KCl unless the in vitro calibrations are carried out in the presence of cell constituents such as aldolase (an abundant myoplasmic protein). Third, under normal resting conditions, $[Ca^{2+}]_r$ in an intact frog fiber appears to lie in the range 0.18–0.27 μM, a range which is somewhat higher than reported in previous studies.

Some of the results have appeared previously in abstract form (36, 37).

METHODS

The tetra-ammonium form of fura red was used exclusively (lot #34111; Molecular Probes Inc., Eugene, OR). Except where noted, all measurements, both in vitro and in vivo, were carried out at 16–17°C.

In vitro measurements

Calibration solutions

(a) Buffer alone. The standard buffer solution contained (in mM): 97.7 KCl, 10 PIPES (piperazine-*N*,*N*'-bis[2-ethane-sulfonic acid]) and either 10 EGTA ('0 Ca^{2+}' solution) or 10 $CaCl_2$ ('sat. Ca^{2+}' solution). The ionic strength was 0.15 M and, unless indicated otherwise, had a pH of 7.03. [Note: all solutions were titrated to a pH of 7.00 at room temperature (~20°C). At 16°C, a solution pH of 7.03 is expected, given the temperature dependence of the PIPES buffer (38)]. For the experiments that characterized the effects of Mg^{2+} on fura red, 10 mM $MgCl_2$ was added to the 0 and sat. Ca^{2+} solutions, resulting in free $[Mg^{2+}]$'s of approximately 8.3 and 10 mM, respectively (assumed apparent dissociation constant of EGTA for Mg^{2+}, 40 mM; cf. reference 39); KCl was lowered to 67.7 mM to maintain ionic strength at 0.15 M. To characterize the effect of pH on fura red, pH was changed to 6.8 (titrated with HCl) or 7.5 (titrated with KOH); as the contribution of PIPES to the total ionic strength is expected to vary with pH, KCl was changed to 100 mM and 93.3 mM, respectively, to maintain ionic strength.

(b) Buffer plus sucrose. To investigate the effects of viscosity on the properties of the indicator (cf. references 3, 32, 40), sucrose was added to the standard buffer solution. The resulting viscosities (reported in centipoise, cP) were: 1.1 cP (no added sucrose), 2.0 cP (0.564 M sucrose) and 2.9 cP (0.842 M sucrose).

(c) Buffer plus aldolase. To investigate possible changes in the properties of fura red associated with the binding of indicator to intracellular proteins, measurements were carried out in the standard buffer solutions with variable concentrations of aldolase, the most abundant soluble protein in myoplasm on a weight basis (41). Rabbit aldolase (type "X"; mol. wt, 160,000; lot #120H9500, Sigma Chemical Co., St. Louis, MO) was dialyzed as described previously (32) to remove Sigma's buffer salts; protein concentration (in mg/ml) was measured by the Bradford method (Coomassie Blue reagent; Pierce Chemical Co., Rockford, IL) with bovine serum albumin (Sigma Chemical, Co.) as standard. Protein solutions were used either immediately after dialysis or stored frozen at −20°C and used within 3 d. The effects of aldolase were assessed in two types of experiments: (*a*) paired measurements that compared the properties of fura red in the standard buffer solution in the absence and presence of aldolase (55 mg/ml protein), for which solution viscosities were 1.1 and 1.6 cP, respectively; (*b*) measurements at different aldolase concentrations (0, 15, 30 and 55 mg/ml), in which solution viscosity was held constant at 1.6 cP by variable additions of sucrose (32).

Absorbance measurements

The absorbance spectrum of fura red (denoted $A(\lambda)$) was measured in a spectrophotometer (Ultraspec 4050; LKB Instruments, Gaithersburg, MD) at wavelengths λ between 400 and 650 nm (λ increments of 2 nm). The spectra were later interpolated to 1 nm resolution and filtered by a smoothing routine that averaged absorbance over 11 adjacent wavelengths. The filtered curves could then be compared with fiber measurements of $A(\lambda)$, which were made on a horizontal optical bench apparatus (42) with interference filters of 10-nm band pass (Omega Optical Co., Brattleborough, VT). Previous in vitro measurements (43) found a negligible difference between $A(\lambda)$ measured in solutions in the spectrophotometer and in glass capillaries mounted on the optical bench apparatus in the same position as the muscle fibers.

Fluorescence measurements

The in vitro fluorescence measurements were carried out with quartz capillaries (i.d., 226 ± 3 μm; Vitro Dynamics, Rockaway, NJ) mounted on the optical bench apparatus. The capillaries were cleaned with EDTA (ethylenedinitrilo-tetraacetic acid) and ethanol and contained indicator at a nominal concentration of 200 μM; a few checks were made with 20 μM indicator. Fluorescence was excited with two wavelength bands, 420 ± 15 nm and 480 ± 15 nm, which are located on either side of the isosbestic wavelength for the Ca^{2+}-fura red reaction (~458 nm). These wavelengths were selected sequentially by interference filters (Omega Optical Co.) inserted manually in the light path between the tungsten-halogen source and the experimental chamber. The length of illuminated capillary, ~300 μm, was determined by the field of view of a long-working-distance objective (Leitz #1569109, 32×, N.A. 0.60) used as a condenser; an identical objective collected the transmitted and fluorescent light from the same length of capillary. Fluorescence emission at wavelengths greater than 550 nm was selected with a barrier filter (KV550; Schott Glass Technologies, Duryea, PA) positioned in the light path between the experimental chamber and the silicon photodiode (UV100; E.G.&G. Inc., Princeton, NJ) used to monitor light intensity. About 1% of the measured intensity was not due to fura red fluorescence but arose because of a small over-lap in the band pass of the excitation and emission filters. The amplitude of this component was estimated separately for both 420 and 480 nm excita-

tion in parallel measurements from capillaries that contained buffer solution without fura red. The raw intensities were corrected for this component to give the fura red fluorescence intensities, denoted F_{420} and F_{480}, respectively. The ratio of F_{420} to F_{480} is denoted R, and the values of R for the Ca^{2+}-free and Ca^{2+}-bound forms of the indicator are denoted R_{MIN} and R_{MAX}, respectively.

Correction for the inner filter effect. For small concentrations of indicator, F_{420} and F_{480} are expected to be linearly proportional to indicator concentration. At larger concentrations, however, fluorescence intensity per unit dye concentration decreases due to the "inner filter effect" (cf. reference 44, p. 443), which arises because the absorption of light by the indicator reduces the intensity of the excitation beam, and possibly also the intensity of the emitted fluorescence, as it moves through the sample. Since fura red's absorbance at the excitation wavelength was usually appreciable in both the in vitro and in vivo measurements, a correction for inner filtering was routinely made. This correction should increase the accuracy of comparisons between in vitro and in vivo fluorescence measurements carried out at different absorbance levels.

Eqs. 1–5 of reference 45 permit a measured fluorescence intensity to be referred to the intensity expected in the absence of reductions due to absorbance. As follows from this theory, the measured fluorescence intensity F is given by:

$$F = k \cdot I \cdot A \cdot \frac{(10^{-B_i - B} - 10^{-A_i - A})}{(A_i + A - B_i - B)}, \qquad (1)$$

where I denotes the intensity of the excitation beam incident on the fiber; k is a constant that depends on the indicator's quantum efficiency for fluorescence and the collection efficiency of the apparatus; A and B denote the absorbance of the indicator at the excitation and emission wavelengths, respectively; and A_i and B_i (i for intrinsic) denote any absorbance of the sample at the excitation and emission wavelengths, respectively, that does not depend on the presence of the indicator. In the case of fura red, B is close to zero since the emission spectrum of the indicator, for both the Ca^{2+}-free and Ca^{2+} bound forms, occurs primarily at longer wavelengths ($\lambda > 570$ nm), where indicator absorbance is negligible (see Fig. 2). Additionally, for the in vitro measurements, A_i and B_i can be assumed to be zero since the absorbance of the buffer solution in the absence of dye is small. To correct then an in vitro measurement of fluorescence intensity F for reductions due to absorbance, F was multiplied by the factor Y_1:

$$Y_1 = \log_e 10 \frac{A}{(1 - 10^{-A})}. \qquad (2)$$

Y_1 has a value greater than 1.0 and, from Eq. 1, refers F to the intensity that would have been measured in the absence of inner filtering.

A was not measured in the capillary calibrations but was calculated with Beer's law: $A = \epsilon \cdot [D_T] \cdot l$ (where ϵ denotes the molar extinction coefficient, $[D_T]$ denotes the indicator concentration, and l denotes the path length through the sample). With both 420 and 480 nm excitation, ϵ varies with f, the fraction of the indicator in the Ca^{2+}-bound form. The effective values of $\epsilon(420)$ and $\epsilon(480)$ were estimated for both the Ca^{2+}-free ($f = 0$) and the Ca^{2+}-bound ($f = 1$) forms of fura red from the relative shapes of the spectrophotometer absorbance spectra reported in Results, the absolute extinction coefficient assumed for the isosbestic wavelength (given below in Methods) and the band-width of the excitation filters (30 nm). From the dye concentration (0.2 mM), the path length (192 μm if averaged over the width of the 226 μm capillary), and the estimated values of ϵ, values of Y_1 were calculated for each of the in vitro calibration solutions discussed in the Results section. The Y_1 values calculated for the two calibration solutions used most commonly were:

(*a*) *2.0 cP, no added aldolase:* for 420 nm excitation, 1.050 if $f = 0$ and 1.122 if $f = 1$; for 480 nm excitation, 1.100 if $f = 0$ and 1.037 if $f = 1$.

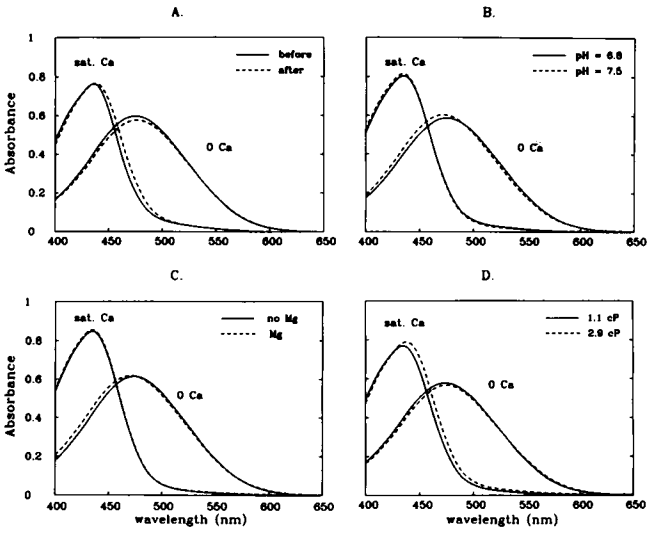

FIGURE 2 Absorbance spectra of fura red in 0 Ca^{2+} and saturating Ca^{2+} solutions. Each panel shows the effect of one variable on the spectra: (*A*) (before and after) 8 min of illumination with white light; (*B*) pH (6.8 and 7.5); (*C*) free $[Mg^{2+}]$ (0 mM for "no Mg" condition; either 8.3 mM (0 Ca spectrum) or 10 mM (sat. Ca spectrum) for "Mg" condition; (*D*) viscosity (1.1 cP, no added sucrose; 2.9 cP, with 0.842 M sucrose). All measurements were made in a spectrophotometer with a 1 cm cuvette that contained a nominal fura red concentration ($[D_T]$) of 25 μM. Although actual concentrations may differ slightly from 25 μM, within any one panel the values of $[D_T]$ should have been identical for all 4 solutions. See Methods for exact solution composition.

(*b*) *1.6 cP, 55 mg/ml aldolase:* for 420 nm excitation, 1.038 if $f = 0$ and 1.106 if $f = 1$; for 480 nm excitation, 1.101 if $f = 0$ and 1.033 if $f = 1$.

Anisotropy. If fura red fluorescence is excited with linearly polarized light, the fluorescence emission anisotropy (denoted a) is defined as (cf. 44):

$$a = \frac{F_\parallel - F_\perp}{F_\parallel + 2F_\perp}, \qquad (3)$$

where $F_\parallel$ and $F_\perp$ denote the components of fluorescence intensity emitted with polarization parallel and perpendicular, respectively, to the excitation beam. The theoretical minimum and maximum values of a are −0.2 and +0.4 (44). Anisotropy at the two excitation wavelengths (denoted $a(420)$ and $a(480)$) was measured by the method previously described (32), with the excitation beam polarized either parallel or perpendicular to the long axis of the quartz capillary. Within the error of the measurements, the anisotropy levels measured with the two polarized excitation beams were identical, as expected for molecules in solution; thus, the in vitro values of a reported in Results represent the average of the two polarized measurements.

Estimation of K_D

Fura red's dissociation constant for Ca^{2+} (K_D) was estimated from absorbance spectra measured in solutions containing the same concentration of fura red (nominally 25 μM) but different free Ca^{2+} concentrations. $[Ca^{2+}]$ was set with 10 mM EGTA as the buffer under the assumption that the apparent dissociation constant of the Ca^{2+}-EGTA reaction for the experimental conditions (16°C; ionic strength of 0.15 M; pH of 7.03) is 0.41 μM (cf. references 38, 46). For each solution that contained a non-zero free $[Ca^{2+}]$, the difference absorbance spectrum ($\Delta A(\lambda)$) was determined by subtraction of the absorbance spectrum of the 0 Ca^{2+} solution. The amplitude of each difference spectrum

was then compared with that of fura red's saturating absorbance change ($\Delta A_{MAX}(\lambda)$), defined as the difference in absorbance between the sat. and 0 Ca^{2+} solutions. Relative spectral amplitude was defined by the scaling constant that provided a least-squares fit of $\Delta A_{MAX}(\lambda)$ to $\Delta A(\lambda)$ over all λ values ($400 \leq \lambda \leq 650$ nm). From the relative amplitude data and the corresponding $[Ca^{2+}]$ levels, K_D was estimated by a least-squares fit of the equation for 1:1 binding (Ca^{2+}:fura red):

$$f = \frac{[Ca^{2+}]}{[Ca^{2+}] + K_D}. \quad (4)$$

f, the fraction of the indicator in the Ca^{2+}-bound form, was identified with the relative amplitude of the difference spectrum estimated at each level of $[Ca^{2+}]$ (cf. Fig. 5 described in detail below).

Measurements with soluble proteins from bullfrog

As a check on how well a buffer solution containing rabbit aldolase may mimic the protein environment of the myoplasmic solution, and specifically on how the properties of fura red might be altered by this environment, a few measurements were carried out with buffer solution to which were added soluble proteins isolated from bullfrog leg muscles. These measurements were carried out by Dr. Kurebayashi in the Department of Pharmacology, Juntendo University. The general procedure for isolation of the muscle components was identical to that described previously (47). After homogenization of the leg muscles, the myofibrillar fraction was removed by low-speed centrifugation (6,000 rpm) and the supernatant was subjected to higher-speed centrifugation (15,000 rpm) to remove the microsomal fraction. The supernatant from this fraction was centrifugally concentrated with Amicon Centriprep-30 (Danvers, MA), which produced a four-fold concentration of the constituents of molecular weight > 30 kD. The final protein concentration of this fraction (referred to below as "soluble proteins") was 45 mg/ml, as determined by the Biuret method. This concentration, if referred to the original muscle weight, corresponded to 3.9 g of soluble protein per 200 g muscle wet weight or, equivalently, 34 mg of soluble protein per ml of myoplasmic water (see reference 48 for unit conversions). By weight, aldolase accounted for ~35% of the soluble proteins, as determined by Coomassie Blue staining on SDS polyacrylamide gel. Fura red optical signals were measured in a buffer solution containing either 0 or 22 mg/ml soluble protein. Absorbance spectra of 25 μM fura red were measured in a Shimadzu UV-160 spectrophotometer (16°C), whereas fluorescence intensities of 2.5 μM fura red were measured in a Hitachi 850 fluorescence spectrophotometer (21–24°C). For fluorescence, 420 nm and 480 nm excitation wavelengths were used (5-nm band pass), with emission measured at 630 nm (also with a 5-nm band pass).

In vivo measurements

The experiments on muscle fibers were carried out on intact single fibers dissected from leg muscles (iliofibularis or semi-tendinosus) of cold-adapted *Rana temporaria*. The methods were similar to those previously described (cf. references 22, 7). The normal Ringer solution used for dissection contained (in mM): 120 NaCl, 2.5 KCl, 5 PIPES and 1.8 $CaCl_2$ (pH = 7.1). An isolated fiber was transferred to the experimental chamber on the optical bench apparatus and bathed either in a "high-Ca^{2+}" Ringer solution (as above, but containing 11.8 instead of 1.8 mM $CaCl_2$) or, less frequently, in the normal Ringer solution. In the high-Ca^{2+} Ringer there was less likelihood of fiber damage from the micro-electrode impalements required for the injection of indicator (cf. reference 49). Except as noted in Results, fibers were stretched to a long sarcomere length, 3.5–4.0 μm, and lowered onto pedestal supports to minimize movement artifacts in the optical measurements. In the first set of experiments, fura red was pressure injected into the fiber from a micro-pipette containing 20 mM fura red dissolved in distilled water. However, injections in this solution were often difficult as the fura red had a tendency to form micro-precipitates, which plugged the electrode tip. In the later experiments, the precipitate formation was reduced by the use of 0.1 M KCl rather than water as the solvating agent. Just prior to the fura red injection, and periodically during the course of an experiment, the fiber's intrinsic birefringence change due to action potential stimulation ("second component" of the birefringence signal; 50) was recorded to assess fiber condition. Fibers were used only if the birefringence signal had a normal amplitude (fractional change in light intensity ≥ 0.001) and time course (time to peak, 8–10 ms after stimulation) when measured from fiber regions that contained ≤0.1 mM fura red (cf. Results). During the data collection runs (see below), the waiting period between single action potentials was ~30 s.

Absorbance measurements. To determine fura red's absorbance in myoplasm, a fiber region was trans-illuminated with a small spot of light, the diameter of which was less than the fiber diameter. Transmitted intensities were measured sequentially, with appropriate bracketing, at wavelengths between 440 and 630 nm, in increments of 10 to 30 nm. Except for λ = 630 nm, the wavelength was selected by two identical interference filters (10-nm band pass; Omega Optical Co.), one positioned before the muscle fiber and one after the muscle fiber in the light path. This simultaneous use of two identical filters prevented the longer wavelength fluorescent light from contaminating the measurement of transmitted intensity. For λ = 630 nm, a wavelength at which fura red has no absorbance, a single interference filter of 30-nm band pass was positioned between the light source and the muscle fiber. The intensity of light transmitted by the fiber in the resting state (denoted $I(\lambda)$) was compared with that measured in the absence of the fiber (denoted $J(\lambda)$) and the apparent absorbance of the fiber, $A_T(\lambda)$, was calculated as previously described (43). In Results, the procedure is illustrated whereby $A_T(\lambda)$ was corrected for the contribution from the fiber's intrinsic absorbance (denoted $A_i(\lambda)$) to yield the indicator-related component (denoted $A(\lambda)$). From the estimated absorbance of the indicator at the isosbestic wavelength for Ca^{2+} (λ_{iso}), Beer's law was used to calculate the total concentration of indicator (denoted $[D_T]$) from the myoplasmic path length, which was estimated from the measured fiber diameter as previously described (43). For this calculation, one of two isosbestic wavelengths and corresponding molar extinction coefficients were assumed: (*a*) λ_{iso} = 458 nm and $\epsilon(458) = 2.1 \times 10^4$ M^{-1} cm^{-1}, or (*b*) λ_{iso} = 459 nm and $\epsilon(459) = 1.87 \times 10^4$ M^{-1} cm^{-1}. These values were estimated, respectively, from spectrophotometer measurements of $A(\lambda)$ in the 2.0 cP solution without aldolase or in the 1.6 cP solution with aldolase (cf. Results) under the assumption that the weight of fura red as supplied by Molecular Probes in their 500 μg vials is accurate.

To estimate f_r, the fraction of fura red in the Ca^{2+}-bound form at rest, the fiber $A(\lambda)$ data were least-squares fitted as a linear combination of two in vitro spectra, one measured in a 0 Ca^{2+} and the other in a sat. Ca^{2+} solution (denoted $A_0(\lambda)$ and $A_{sat}(\lambda)$, respectively; cf. Fig. 7 and associated discussion). f_r was converted to $[Ca^{2+}]_r$ by means of Eq. 4 after assumption of a particular value of K_D.

In conjunction with the resting measurement of $I(\lambda)$, the fractional change in transmitted intensity (denoted $\Delta I/I$; λ's also between 440 and 630 nm) was measured following an action potential, which was stimulated locally by a suprathreshold shock from a pair of extracellular electrodes. In order to obtain the fura red-related signal, $\Delta I/I$ at each λ was first corrected for a component due to an intrinsic change of the fiber and then calibrated in ΔA units ($= -(1/\log_e 10)\Delta I/I$), a procedure also illustrated in the Results section. Beer's law was then used to convert ΔA to Δ[CaD], the change in concentration of Ca^{2+}-fura red complex. For this purpose, one of two values was assumed for the change in fura red's molar extinction coefficient with Ca^{2+} complexation: (*a*) $\Delta\epsilon(494) = 1.71 \times 10^4$ M^{-1} cm^{-1} or (*b*) $\Delta\epsilon(498) = 1.97 \times 10^4$ M^{-1} cm^{-1}. These values were also estimated from the spectrophotometer data and correspond, respectively, to the 2.0 cP condition and the aldolase condition mentioned above for calculation of $[D_T]$.

Fluorescence measurements. Fluorescence intensities in resting muscle fibers (denoted F_{420} and F_{480}) were measured by the same technique

used for the quartz capillary measurements. In the analysis stage, the F values were also corrected for reductions in intensity due to absorbance (cf. Eq. 1 above and Eq. 5 below). F measurements were always carried out in a bracketed fashion (F_{420}, then F_{480}, then F_{420}) and the two values of F_{420} were averaged prior to comparison with F_{480}. In most experiments, F_{420} and F_{480} were measured from several fiber regions, each located a different distance from the site of fura red injection. For any particular measurement, the axial length of fiber illuminated was ~70 μm, as determined by a slit positioned in the light path and oriented transversely to the fiber axis. The short illuminated length reduced any axial variations in $[D_T]$ and $[Ca^{2+}]_r$ within the measurement region. $[D_T]$ varied because of the slow time course for diffusion of indicator away from the site of injection, whereas $[Ca^{2+}]_r$ varied in some fibers because of injection damage, which tended to elevate $[Ca^{2+}]_r$, and possibly because of complexation of Ca^{2+} by the indicator, which tended to lower $[Ca^{2+}]_r$. The non-fura red component of intensity was estimated in each experiment and for each excitation wavelength after axial translation of the fiber to a location distant (e.g., 1.5–2.0 mm) from the injection site, where $[D_T]$ was zero. As a fraction of the raw intensity measurement, the amplitude of the non-fura red component depended on $[D_T]$ and was typically 0.005–0.05 (for the usual measurement locations, which were located within 0.6 mm of the injection site).

Changes in F_{420} and F_{480} in response to an action potential (denoted ΔF_{420} and ΔF_{480}) were also measured. As for F_{420} and F_{480}, ΔF_{420} and ΔF_{480} were determined in a bracketed fashion and the two ΔF_{420} measurements were averaged prior to comparison with ΔF_{480}. Each ΔF measurement was always immediately preceded by a measurement of resting F so that the fractional change in fluorescence ($\Delta F/F$) could be determined. The ΔF signals were also recorded from fiber regions located at different distances from the injection site.

Each in vivo measurement of F was multiplied by a correction factor (denoted Y_2) that referred F to the intensity that would have been measured in the absence of reductions due to the absorbance of light by the fiber:

$$Y_2 = \log_e 10 \frac{(A + A_i - B_i)}{10^{-B_i} - 10^{-A_i - A}}. \quad (5)$$

Y_2, like Y_1 (cf. Eq. 2) is greater than 1.0 and corrects for the reduction in F due to A, the indicator-related absorbance. Y_2, in contrast to Y_1, also corrects for reductions in F due to A_i and B_i, which, for a muscle fiber, are small but not entirely negligible. For typical values of A, A_i and B_i encountered in muscle fibers, Y_2 was 10–15% larger than Y_1. The use of Y_2 rather than Y_1, however, had a much smaller influence on the calibration of $[Ca^{2+}]_r$ from the fluorescence ratio signal. This arises because the ratio of the correction factor at 420 nm to that at 480 nm, which is what mainly influences the calibration of the fluorescence ratio signal, was typically only 1–2% larger for Y_2 than for Y_1. B_i was approximated for each fiber by the intrinsic absorbance measured at 630 nm (range of values, 0.027–0.046; cf. Results), whereas A_i was approximated as the intrinsic absorbance of the fiber at the central wavelength of the relevant excitation band (420 or 480 nm; range of estimated values, 0.044–0.075 and 0.037–0.064, respectively; see legend of Fig. 7 for the method of estimation of A_i). For a fiber region from which both absorbance and fluorescence measurements were made ("primary" location), A in Eq. 5 was determined directly as described in the preceding section; for other fiber regions ("secondary" locations), A was calculated from the value of A measured at the primary location and the relative values of F measured at the primary and secondary locations. In the latter case, iteration was used to obtain estimates of Y_2 and A that were consistent with Eq. 5 and the measurements at the primary location.

Correction of the ΔF's measured during fiber activity was also carried out by similar methods. During activity, Y_2 changed continuously with time, although in a minor way. At a primary location, the change in Y_2 could be calculated directly from Eq. 5 and the measured ΔA (cf. Figs. 8–9); for a secondary location, the change in Y_2 was calculated indirectly, from the absorbance change inferred from the fluorescence change. Sample values of Y_2, both at rest and during activity, are given in the legends of Figs. 8 and 11.

R, the fluorescence ratio signal from the fiber, was determined under two conditions: at rest ($R_r = F_{420}/F_{480}$) and following action potential stimulation ($R' = (F_{420} + \Delta F_{420})/(F_{480} + \Delta F_{480})$). Conversion of the ratio signals to $[Ca^{2+}]$ levels was carried out as a two-step process: (*a*) an appropriate in vitro calibration curve was selected to permit conversion of R to f; then (*b*) Eq. 4 was applied after assumption of a particular value of K_D.

Software. Data analysis and figure preparation were carried out either (*a*) on a PDP-11 computer with programs written in Fortran, or (*b*) on AT-compatible computers with MLAB (Civilized Software, Bethesda, MD), a high-level mathematics and curve-fitting program.

Statistics. Unless stated otherwise, results collected from more than two experiments are reported as means ± standard error of the mean (± SEM). Statistical differences were evaluated with Student's two-tailed t-test at $P < 0.05$.

RESULTS

Part I: In vitro measurements

Effects of illumination on fura red

In preliminary measurements it was noticed that, with fura red in the standard buffer solution, F_{420} and F_{480} decreased if the solution was exposed to the usual light intensities available from the 100 W tungsten-halogen source on our optical bench apparatus. For example, if $F_{420}(t)$ denotes the (normalized) value of F_{420} measured immediately after t seconds of steady illumination with 420 nm light, the following values were observed for Ca^{2+}-free fura red: $F_{420}(0) = 100\%$, $F_{420}(20) = 90\%$, $F_{420}(40) = 88\%$, $F_{420}(60) = 87\%$ and $F_{420}(300) = 85\%$. Somewhat larger and more rapid changes were observed for Ca^{2+}-bound fura red: $F_{420}(0) = 100\%$, $F_{420}(20) = 67\%$, $F_{420}(40) = 66\%$, $F_{420}(60) = 65\%$ and $F_{420}(300) = 63\%$. These changes in fluorescence intensity are qualitatively similar to changes described for fura-2 during a 25 s illumination with ultraviolet wavelengths (51). As described below, however, the principal effects on fura red that we have detected following several min (typically 5 min, range 2–10 min) of illumination with visible light are quite different from the effects on fura-2 described in reference 51 following 2–30 min of illumination with UV radiation.

Because fluorescence intensities of fura red appeared to be stabilized by a period of steady illumination, the principal measurements described in this paper were carried out with dye solutions that had been preilluminated with white light for several minutes. Interestingly, the mechanism whereby fura red is converted by light to a less fluorescent species does not appear to be a simple bleaching of the indicator. This is shown in Fig. 2 *A*, which compares absorbance spectra of fura red measured before and after 8 min of steady illumination. With illumination, there were minimal changes in absorbance: the Ca^{2+}-free spectrum appeared to decrease slightly (~3%) in amplitude, without a detectable wave-

length shift, whereas the Ca^{2+}-bound spectrum was red-shifted slightly (~3–4 nm for wavelengths between 450 and 600 nm), without a significant change in amplitude. As a result, a small red-shift was observed in the indicator's isosbestic wavelength for Ca^{2+} (from ~455 nm to ~458 nm). Since the substantial change in the fluorescence of fura red produced by illumination was not accompanied by a comparable change in the absorbance of the indicator, the chemical alteration induced by light probably involves a photo-isomerization (not a bleaching) of the compound (see the discussion in reference 3 concerning photo-isomerization of stilbene groups). The carbon atom about which the isomerization is presumed to occur is indicated by the arrow in Fig. 1 *B*.

Other properties of fura red were also minimally affected by several min of illumination with white light. For example, the indicator's K_D for Ca^{2+} was estimated to be 0.38 μM before illumination and 0.39 μM after illumination. R, the indicator's fluorescence ratio signal, also changed relatively little. In 10 measurements from 4 solutions, prior to illumination R_{MIN} varied between 0.15 and 0.16 and R_{MAX} varied between 1.42 and 1.58, whereas after illumination, R_{MIN} varied between 0.15 and 0.16 and R_{MAX} between 1.46 and 1.62.

Although fura red's fluorescence intensity levels were more stable if the indicator had been preilluminated with white light, intensity levels were not completely stabilized by the illumination. For example, for Ca^{2+}-bound fura red that had been preilluminated, a series of 10 measurements of F_{420}, taken at 2 s intervals, with each measurement exposing the indicator to 420 nm light for ~0.5 s, revealed 5–9% decrements between the first and last measurements in the series of 10 (9 series from 5 solutions). These decrements were, however, considerably smaller than the 25–30% decrements observed during analogous measurements taken without preillumination of the indicator (9 series from 3 solutions). Ca^{2+}-free fura red that had been preilluminated appeared more stable, with a decrement of ~1% detected during a similar series that examined F_{480}. For comparison, decrements of 5–7% were observed in analogous measurements of F_{480} taken without preillumination of the indicator (8 series from 3 solutions).

Interestingly, if Ca^{2+}-bound fura red, but not Ca^{2+}-free fura red, had been preilluminated with white light, a 10–20 s exposure to 480 nm light produced *increases* in F_{420} of 30–35% and in F_{480} of 17–23% (3 measurements from 2 solutions); the corresponding change in R_{MAX} was an increase that varied between 9 and 15%. In the case of F_{420}, the final levels after the 10–20 s exposure to 480 nm light were closer to, but still 10–15% less than, the initial levels measured before the illumination with white light. (In these experiments, the levels of F_{480} prior to illumination were not measured.) Thus, for F_{420} at least, the decrease in fluorescence intensity of Ca^{2+}-bound fura red induced by white light was largely, although perhaps not entirely, reversed by subsequent illumination with 480 nm light. Again, changes of this sort are consistent with a photo-isomerization (not a bleaching) of the compound.

Surprisingly, the fluorescence of Ca^{2+}-bound fura red was stabilized by the presence of 55 mg/ml aldolase. For example, in the presence of aldolase, exposure of fura red (preilluminated with white light) to 480 nm light increased F_{480} by only 3%, compared with the 17–23% increase noted in the absence of aldolase. (We did not separately determine whether the initial reduction in intensity caused by the preillumination with white light was affected by aldolase.) It is of interest to note that measurements on dye-injected muscle fibers (see Results, Part II) revealed no detectable effects of illumination per se on fura red's fluorescence. This finding is probably related to the stabilizing effect that protein (e.g., aldolase) has on fura red's fluorescence, since, in the fiber, a large fraction of fura red appears to be bound to relatively immobile constituents such as soluble proteins (see Results, Part II).

In order to minimize light-induced changes in the fluorescence intensity of fura red, the remaining measurements described in this article, both in vitro and in vivo, were made on indicator that had been preilluminated with white light.

Effects of Ca^{2+}, pH and Mg^{2+} on absorbance

Ca^{2+}. As shown in Fig. 2, the absorbance spectrum of fura red undergoes a large change as a result of Ca^{2+} complexation, with an increase in peak amplitude of ~30% and a shift in location of the peak, from ~476 nm in the absence of Ca^{2+} to ~437 nm in the presence of Ca^{2+}. These changes are qualitatively similar to those seen with fura-2 except that, with fura-2, the absorbance peaks occur at wavelengths less than 400 nm (3, 32).

pH and Mg^{2+}. In general, for indicators of the tetracarboxylate family, changes in pH or Mg^{2+} in the physiological range are expected to have little effect on either the compound's spectral properties or its K_D for Ca^{2+} (1, 3). As shown in Fig. 2, fura red's absorbance in both its Ca^{2+}-free and Ca^{2+}-bound forms is quite insensitive to pH levels between 6.8 and 7.5 (panel *B*) or free Mg^{2+} levels between 0 and 8.3 mM (panel *C*). To the extent that effects of pH and Mg^{2+} occur, they appear larger for the Ca^{2+}-free than for the Ca^{2+}-bound form of the indicator.

Effects of Ca^{2+}, pH and Mg^{2+} on fluorescence

Each part (A–D) of Table 1 shows fluorescence signals (F_{420}, F_{480} and R) measured on a particular day under various solution conditions. Cols. 1–3 give information for the Ca^{2+}-free form of the indicator and columns 4–6 for the Ca^{2+}-bound form. Within each part of the Table, intensities are given relative to that of F_{480} measured in a 0 Ca^{2+} solution under a standard condition (16°C; pH = 7.03, $[Mg^{2+}] = 0$, viscosity = 1.1 cP; see 4 rows marked with an asterisk). For this condition, the following aver-

TABLE 1 **In vitro fluorescence in 0 and saturating Ca^{2+} solutions**

	0 Ca^{2+}			Sat. Ca^{2+}		
	F_{420} (1)	F_{480} (2)	R_{MIN} (3)	F_{420} (4)	F_{480} (5)	R_{MAX} (6)
A. pH						
6.8	0.136	0.997	0.136	0.210	0.129	1.628
7.0*	0.142	1.000	0.142	0.205	0.123	1.667
7.5	0.164	1.068	0.154	0.198	0.121	1.636
B. Mg^{2+}						
0 mM*	0.142	1.000	0.142	0.214	0.134	1.597
8.3 mM	0.151	0.937	0.161	—	—	—
10 mM	—	—	—	0.211	0.133	1.586
C. Viscosity						
1.1 cP*	0.143	1.000	0.143	0.239	0.136	1.757
2.0 cP	0.224	1.641	0.137	0.368	0.287	1.282
2.9 cP	0.274	2.037	0.135	0.454	0.401	1.132
D. Aldolase						
0 mg/ml*	0.152	1.000	0.152	0.226	0.130	1.738
55 mg/ml	0.452	4.406	0.103	1.023	1.483	0.690

Relative fluorescence intensities (F_{420}, F_{480}) and fluorescence ratios (R_{MIN}, R_{MAX}) are shown for different conditions of pH (*A*), Mg^{2+} (*B*), viscosity (set with sucrose) (*C*) and aldolase (*D*). The solutions marked with an asterisk denote identical solution composition (0 mM Mg^{2+}; pH of 7.03; 1.1 cP, i.e., no added sucrose or aldolase). For each condition (*A–D*), the measurements were carried out on the same day with solutions containing identical fura red concentrations (nominally 0.2 mM); the intensity data for that condition have been normalized by the F_{480} value of the 0 Ca^{2+} solution with the asterisk. All *F* measurements reported here and elsewhere in the paper have been corrected for the inner filter effect (see Methods).

age changes ($N = 4$) were observed with Ca^{2+} complexation: an increase in F_{420} from 0.145 to 0.221, a decrease in F_{480} from 1.000 to 0.131 and an increase in R from an R_{MIN} of 0.145 to an R_{MAX} of 1.690. Parts *A* and *B* of Table 1 show that levels of pH and Mg^{2+} in the physiological range have relatively small effects on the fluorescence signals.

Effects of viscosity on absorbance and fluorescence

Absorbance. Fig. 2 *D* shows that an increase in viscosity from 1.1 to 2.9 cP produced little change in the absorbance spectrum of Ca^{2+}-free fura red (perhaps a decrease in amplitude of 1–2%) and a slightly greater change for that of Ca^{2+}-bound fura red (an increase in amplitude of 2–3% and a red-shift of ~3 nm). In terms of the isosbestic wavelength for Ca^{2+}, there was a small red-shift (from ~456 nm to ~460 nm). Although the viscosity of myoplasm is not known precisely, previous work suggests that it is probably about 2 cP at 20°C (52). For characterization of a number of in vivo measurements described in Part II of Results, we have used the average of the absorbance spectra measured in the 1.1 and 2.9 cP solutions (0 and sat. Ca^{2+} spectra averaged separately); we refer below to these spectra as "2.0 cP" spectra.

Fluorescence. Part *C* of Table 1 summarizes fluorescence measurements at three viscosities (1.1, 2.0 and 2.9 cP). With the exception of R_{MIN}, the fluorescence signals were affected substantially by viscosity. For example, intensity levels were 2–3 times larger at 2.9 cP than at 1.1 cP. These effects are seen more clearly in Fig. 3. The filled circles in Fig. 3 *A* show F_{420} and F_{480} measured in the 1.1 and 2.9 cP solutions, both for 0 Ca^{2+} ($f = 0$) and sat. Ca^{2+} ($f = 1$) conditions. The lines in Fig. 3 *A* connect the 0 and sat. Ca^{2+} data points for otherwise comparable measurements. Under the assumption that a fura red molecule is either Ca^{2+}-free or Ca^{2+}-bound, these lines predict the fluorescence levels for intermediate values of f. The curves in Fig. 3 *B* were obtained as the ratio of the lines in Fig. 3 *A* (420 divided by 480) and show the relationship between R and f for the 1.1 and 2.9 cP conditions. Since increasing viscosity significantly lowers R_{MAX} but not R_{MIN}, there is a substantial decrease in the curvature of the relationship between R and f at the higher viscosity. Although the 2.0 cP data are not plotted in Fig. 3 *A* and Fig. 3 *B*, the corresponding lines and curve fell between the 1.1 and 2.9 cP cases shown (cf. part *C* of Table 1).

Effects of 55 mg/ml aldolase

Previous in vitro studies with fura-2 (32, 53) found that soluble proteins from myoplasm (e.g., aldolase, creatine kinase, glyceraldehyde-3-phosphate dehydrogenase, lactic dehydrogenase) as well as from other sources (e.g., bovine serum albumin), if included in the calibration solutions at concentrations comparable to the total soluble protein concentration of myoplasm (50–90 mg/ml; 41), had a major effect on fura-2's properties. Moreover, a number of properties of fura-2 observed in muscle fibers are consistent with the idea that fura-2 is heavily bound to myoplasmic proteins and that this binding alters indicator properties in the approximate manner observed in the in vitro calibrations (7, 32). It was there-

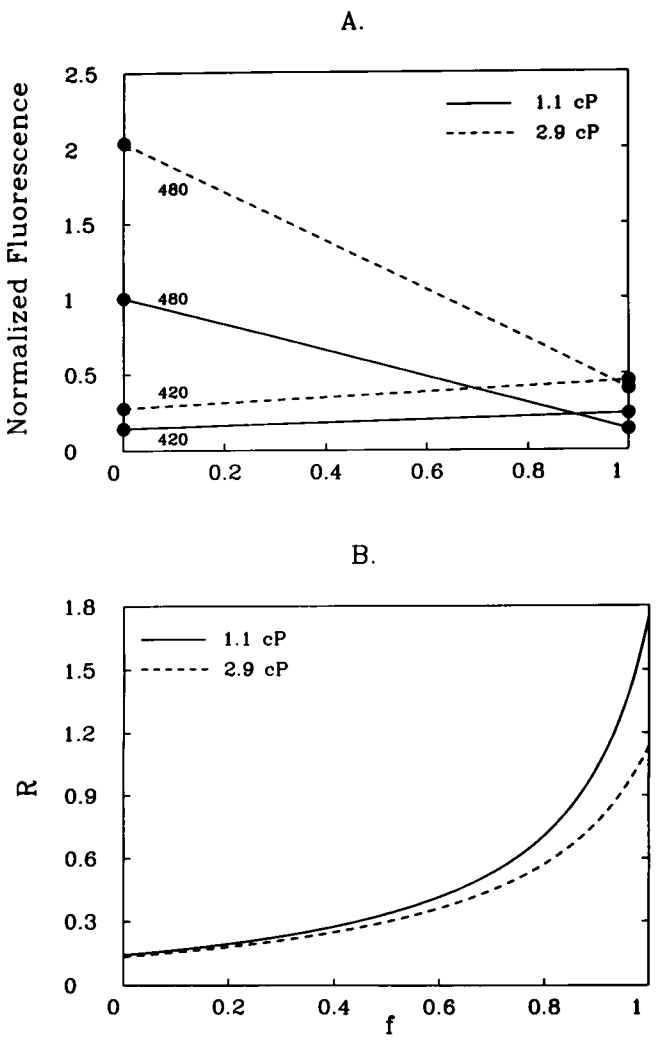

FIGURE 3 In vitro fluorescence signals (ordinate) as a function of f, the fraction of fura red in the Ca^{2+}-bound form (abscissa). (*A*) Fluorescence intensity of fura red, measured with two excitation wavelengths (420 and 480 nm), at two viscosities (1.1 and 2.9 cP), and for two levels of Ca^{2+}: 0 Ca^{2+} ($f = 0$) and saturating Ca^{2+} ($f = 1.0$). The eight intensity values (filled circles) have been normalized by the value of F_{480} measured at 1.1 cP in 0 Ca^{2+}; the values at 0 and sat. Ca^{2+} for otherwise identical conditions have been connected by line segments (continuous lines for 1.1 cP; dashed lines for 2.9 cP). (*B*) The fluorescence ratio signal R ($=F_{420}/F_{480}$) obtained from the ratio of the lines in *A* at each of the viscosity values.

fore of interest to determine whether the properties of fura red are similarly affected by soluble muscle proteins. A number of in vitro properties of fura red were therefore measured in the absence and presence of aldolase, the most abundant soluble protein in myoplasm on a weight basis (41). A few measurements were also made with a soluble protein fraction isolated from bullfrog leg muscles (cf. Methods) to check whether the effects detected with aldolase appeared to be representative of the soluble protein fraction.

Absorbance. Fig. 4 *A* compares absorbance spectra (0 Ca^{2+} and sat. Ca^{2+}) measured under standard conditions in the absence of protein (*continuous curves;* viscosity = 1.1 cP) and in the presence of 55 mg/ml aldolase (*dashed curves;* viscosity = 1.6 cP). With aldolase, the peak of the 0 Ca^{2+} spectrum was red-shifted by about 12 nm, without a significant change in amplitude, whereas the sat. Ca^{2+} spectrum was red-shifted only slightly (~3 nm) while its amplitude decreased by ~10%. The Ca^{2+}-difference spectra determined by the spectra in Fig. 4 *A* are shown in Fig. 4 *C*. With aldolase, there was a slight change in shape of the difference spectrum and a small red shift in the isosbestic wavelength (from ~456 nm to ~459 nm). On the long wavelength side of the difference spectrum ($\lambda > 500$ nm), where absorbance changes during muscle activity are very accurately resolved in our apparatus (cf. 29), the aldolase-induced red-shift in the difference spectrum is substantial, 6–7 nm.

Fluorescence. Part *D* of Table 1 and panels *B* and *D* of Fig. 4 show the effect of 55 mg/ml aldolase on F_{420}, F_{480} and R. Large effects are seen, much larger than expected based on the relatively small difference in the viscosity of the solutions (1.6 vs. 1.1 cP). The effects are also much larger than predicted from the relatively minor effects of aldolase on the indicator's absorbance spectra (Fig. 4 *A*). With aldolase, fluorescence intensities increased between 3- and 11-fold, the exact factor depending on both the excitation wavelength and the [Ca^{2+}] level in the solution. Although aldolase must have caused a general increase in the quantum efficiency of fura red's fluorescence, a comparison of panels *A* and *B* of Fig. 4 reveals

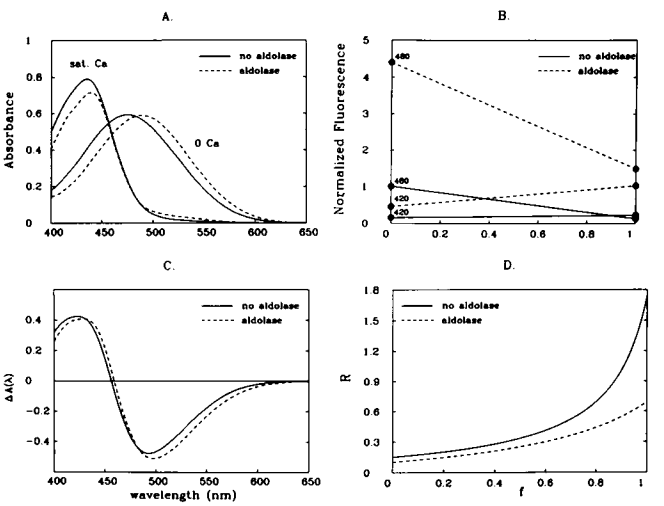

FIGURE 4 (*A*) Fura red's absorbance spectra measured in 0 Ca^{2+} and sat. Ca^{2+} solutions, both with and without 55 mg/ml aldolase (dashed and continuous lines, respectively). The nominal fura red concentration was 25 μM and solution viscosity was 1.6 cP (with aldolase) and 1.1 cP (without aldolase). (*C*) Fura red difference spectra (sat. Ca^{2+} minus 0 Ca^{2+}) obtained by point-by-point subtraction of the spectra in *A* obtained at the same aldolase concentration. (*B*, *D*) Fluorescence intensities and fluorescence ratio signals of fura red in solutions with and without 55 mg/ml aldolase. Presentation details are analogous to those described in the legend of Fig. 3.

that aldolase likely altered the shape of the indicator's fluorescence excitation spectrum; for example, for the Ca^{2+}-bound form of the indicator ($f = 1$), $F_{420} > F_{480}$ in the absence of aldolase but $F_{420} < F_{480}$ in the presence of aldolase. As shown in Fig. 4 *D*, aldolase also changed the fluorescence ratio signal, with substantial decreases in R_{MIN} (by ~30%), R_{MAX} (by ~60%) and in the curvature of the R vs. f relationship. If changes of the magnitude observed in Fig. 4 *D* occur intracellularly, the accuracy of $[Ca^{2+}]_r$ estimated from fura red's fluorescence ratio signal would obviously depend strongly on the method chosen to calibrate the ratio signal.

Estimation of the Ca^{2+}:fura red dissociation constant. In Fig. 5 the symbols show the relative amplitude of fura red's difference absorbance spectrum (*ordinate*) at different values of pCa (*abscissa*). Amplitude data are shown for two conditions (no aldolase, *filled circles;* 55 mg/ml aldolase, *open circles*) and have been normalized by the amplitude observed in a solution with a pCa of ~2. To estimate the apparent dissociation constant of the Ca^{2+}:fura red reaction (denoted K_D) for the two conditions, each data set was separately fitted by the binding curve for 1:1 stoichiometry (cf. Eq. 4). In the absence of aldolase, K_D was ~0.36 μM (*continuous curve*) whereas, in the presence of aldolase, K_D was ~1.59 μM (*dashed curve*). Thus 55 mg/ml aldolase increased K_D ~4-fold. This increase is similar to that previously reported for fura-2, where K_D was ~0.19 μM in the absence of aldolase and ~0.69 μM in the presence of 55 mg/ml aldolase (32; see also 53). [Note: the large increase in fura red's K_D with aldolase is not likely to be due to the small increase in solution viscosity (from 1.1 to 1.6 cP), since previous measurements with fura-2 (32) indicated that a viscosity increase from 1 to 2 cP by itself increased K_D by less than 15%].

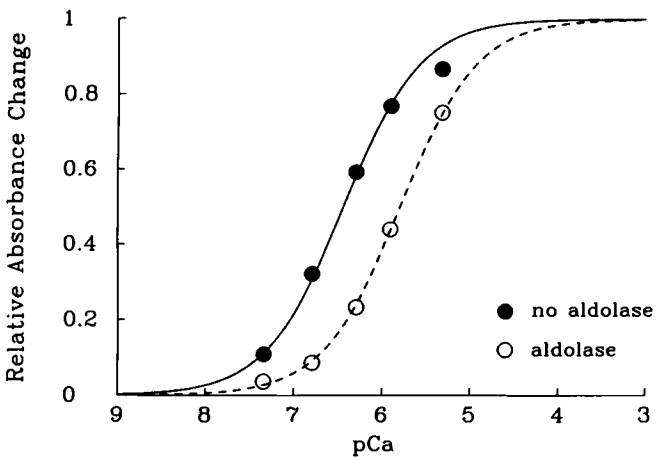

FIGURE 5 The symbols show the relative amplitude of fura red's Ca^{2+} difference spectrum measured in solutions of different pCa, both for the case of no aldolase (filled symbols) and for 55 mg/ml aldolase (open symbols); solution viscosity was 1.1 cP and 1.6 cP, respectively. For each data set, absorbance amplitudes were divided by ΔA_{MAX}, the absorbance change observed at a pCa of ~2 (see Methods). Within any one data set, the shapes of all difference spectra were essentially identical, so that relative amplitudes could be determined by a least-squares fit of the smaller difference spectra with the difference spectrum obtained at pCa = 2. Each curve is the least-squares fit of a 1:1 binding curve to a given data set; the best-fit K_D's were 0.36 μM without aldolase and 1.59 μM with aldolase.

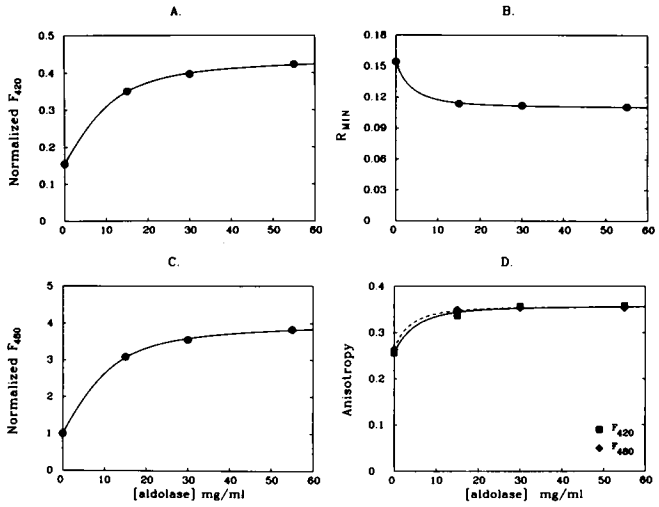

FIGURE 6 Fura red fluorescence measurements (symbols) were made in the presence of different concentrations of aldolase (0 to 55 mg/ml) in a 0 Ca^{2+} solution containing 200 μM fura red. All solutions had a viscosity of 1.6 cP, achieved by variable additions of sucrose (from 0.367 M at 0 mg/ml aldolase to 0 M at 55 mg/ml aldolase). The curves are least-squares fits of the data by the theories described in the text. (*A* and *C*). Fluorescence intensities (F_{420} and F_{480}, respectively) relative to the value of F_{480} measured at 0 mg/ml aldolase. (*B*) R_{MIN}, the fluorescence ratio signal (F_{420}/F_{480}), obtained from the data in panels *A* and *C*. (*D*) Fluorescence anisotropy at two excitation wavelengths, 420 nm (squares and continuous curve) and 480 nm (diamonds and dashed curve).

Concentration-dependence of aldolase effects on fura red

Table 1 and Figs. 4–5 suggest that, in 55 mg/ml aldolase, a significant fraction of fura red is bound to the protein. It was therefore of interest to make measurements at other aldolase concentrations to further characterize the interaction of aldolase and fura red.

Fluorescence intensity and estimation of the aldolase:fura red dissociation constant. The filled circles in panels *A* and *C* of Fig. 6 show relative values of F_{420} and F_{480}, respectively, measured in a 0 Ca^{2+} buffer solution containing different concentrations of aldolase. As expected from Fig. 4 *B*, intensities increase with increasing concentrations of aldolase. The data indicate that the increase in intensity is nearly saturated at 55 mg/ml aldolase and suggest that, at 9 mg/ml, approximately half of the fura red (100 μM out of the 200 μM total) was protein bound. The curves in panels *A* and *C* are a least-squares fit of the data by a theory that estimates the dissociation constant of the aldolase:fura red reaction. This theory is identical to that first applied to analogous data

obtained with fura-2 (32) and assumes that each aldolase molecule can independently bind up to N indicator molecules at equivalent sites characterized by a single dissociation constant (denoted K). In the case of fura-2, a best fit to the data was obtained with an N of 3 and a K of 66 μM.

In applying the theory to the data in panels A and C of Fig. 6, N was set equal to 3, the value previously estimated for fura-2; then a computer program performed a least-squares adjustment of three parameters: K, and the F_{420} and F_{480} values at saturating aldolase, i.e., where all the fura red molecules would be protein bound. The fit yielded a K of 69 μM and saturating levels of F_{420} and F_{480} that were 2.9 and 4.0 times, respectively, the levels measured at 0 mg/ml aldolase. The theoretical curves in panels A and C of Fig. 6 correspond to these parameter selections. Although measurements analogous to those in Figs. 6 A and 6 C were not made in sat. Ca^{2+} solutions, it would be expected from the result in Fig. 5 and the law of mass action that Ca^{2+}-bound fura red would react with aldolase with approximately 4-fold lower affinity (cf. 32), i.e., with a K of $\sim$280 μM (if $N = 3$).

Since aldolase is a homotetramer, it was also of interest to estimate K under the assumption that $N = 4$. In this case a fit with a slightly smaller sum-of-squares deviation was obtained (fit not shown) and the estimated value of K was 121 μM.

Dependence of R_{MIN} on aldolase concentration. The filled circles in Fig. 6 B are the values of R_{MIN}, calculated as the ratio of the F_{420} and F_{480} data points in panels A and C. The curve in panel B was calculated as the ratio of the curves in panels A and C. According to the curve in panel B, the value of R_{MIN} in the presence of saturating protein concentration is $\sim$30% smaller than the value in a protein-free solution (0.110 and 0.155, respectively). In panel B, the half-saturating aldolase concentration (the total aldolase concentration where the corresponding value on the ordinate is the average of the 0 mg/ml value and the saturating value) is $\sim$3.0 mg/ml. As determined by the estimate of K from the fit in panels A and C, of the total fura red only 0.20 (i.e., 40 μM) was bound to aldolase at 3.0 mg/ml.

Anisotropy

If fura red behaves like fura-2 (32), its fluorescence anisotropy, a, should increase with increasing aldolase concentration, an effect explained by a decrease in the rotational mobility of the indicator with protein binding (cf. 44). The data points in panel D of Fig. 6 show that an increase in a was observed at both excitation wavelengths (420 nm, *squares;* 480 nm, *diamonds*). The increase in a occurs even though the indicator is expected to have a longer fluorescence lifetime when in the protein-bound form (cf. the increase in F_{420} and F_{480} observed in Figs. 6 A and 6 C with increasing aldolase concentration; see reference 32 for a similar effect with fura-2), a change that by itself would be expected to reduce anisotropy (44). Evidently, the expected effect on a due to the alteration in fluorescence lifetime is more than compensated by the reduction in rotational mobility of the indicator.

The theoretical curves in Fig. 6 D are also based on a previous theory (32), which assumes that dye can be either in the protein-free form (state 1, with corresponding anisotropy level a_1) or in the protein-bound form (state 2, with corresponding anisotropy level a_2). The measured value of a should then be given by:

$$a = \frac{(1 - f_2)a_1 + pf_2a_2}{(1 - f_2) + pf_2}, \qquad (6)$$

where f_2 denotes the fraction of fura red in state 2 and p denotes the ratio of fluorescence intensity in state 2 to that in state 1. At each of the two wavelengths (420 and 480 nm), the curve in Fig. 6 D was calculated from Eq. 6 after (a) conversion of f_2 to aldolase concentration units by means of the parameters described in connection with the fit in panels A and C of Fig. 6, and (b) adjustment of the parameter a_2 to give a least-squares fit of the functional form to the data. The value of a_1 used in the fit was the corresponding value measured at 0 mg/ml aldolase; the value of p used in the fit, 2.9 and 4.0 for the 420 and 480 nm data, respectively, was the value determined from the fits in panels A and C of Fig. 6. (These latter values estimate the increases in F_{420} and F_{480} with protein binding; see above). The values of a_2 derived from the fits were 0.358 (420 nm data) and 0.357 (480 nm data), whereas the aldolase concentrations at half-saturation were 4.0 mg/ml (at 420 nm) and 3.1 mg/ml (at 480 nm). It is expected that the latter values are less than the 9 mg/ml value obtained from the fits in Fig. 6 A, C, at which half the fura red is estimated to be protein-bound, since the values of p used in Eq. 6 are greater than 1.

Effects of soluble proteins from bullfrog on fura-red properties

Several checks were carried out to see if the soluble protein fraction from bullfrog muscle altered the properties of fura red in a manner similar to that described above for rabbit aldolase. These measurements were made in the standard buffer solution with and without 22 mg/ml protein. Although the concentration of soluble proteins used for these measurements was somewhat smaller than used for most of the aldolase measurements described above (55 mg/ml), the concentration dependence of the aldolase effects noted in Fig. 6 suggests that 22 mg/ml protein should be associated with a near-saturating change in fura red properties.

Absorbance spectra. In a 0 Ca^{2+} solution, fura red's absorbance spectrum was red-shifted about 10 nm by the soluble proteins, while the amplitude of the spectrum decreased slightly ($\sim$7%; spectra not shown). The red-shift was thus quite similar to the 12 nm red-shift seen with 55 mg/ml aldolase. In the sat. Ca^{2+} solution, the

relative amplitudes and shapes of the absorbance spectra with and without soluble proteins were very similar to those shown in Fig. 4 *A* with and without aldolase. In terms of the Ca^{2+}-difference spectrum, soluble proteins produced a small red-shift in the isosbestic wavelength (from 457 to 461 nm), a change very similar to that described in connection with Fig. 4 *A* for the effect of aldolase (where the isosbestic wavelength shifted from 456 to 459 nm).

Fluorescence intensity. In the 0 Ca^{2+} solution, addition of soluble proteins increased fluorescence intensity by 2.8-fold if excited with 420 nm and 8.9-fold if excited with 480 nm light. In the sat. Ca^{2+} solution, fluorescence intensities increased 2.5-fold and 12.1-fold, respectively. The effects of soluble proteins on fluorescence intensity were therefore qualitatively similar to those described above for aldolase (cf. part *D* of Table 1).

Overall, for the parameters measured, soluble bullfrog proteins and rabbit aldolase affected fura red properties in similar ways. Thus in vitro measurements made in the presence of aldolase would appear to represent a reasonable first estimate of indicator properties in the protein environment of myoplasm. In Part II of Results, calibrations in the presence of aldolase and calibrations in a 2.0 cP solution without aldolase were used as the two principal in vitro conditions with which fura red measurements from muscle fibers were compared.

Part II: In vivo measurements

Signals reflecting the cytoplasmic mobility of fura red

Diffusion coefficient. If fura red within the fiber is not bound to intracellular constituents, the diffusion of the indicator along the fiber axis should be described by a diffusion coefficient predictable from the molecular weight of the compound. For fura red (MW of 652 for the tetravalent anion) the diffusion coefficient at 16°C is expected to be about 1.0×10^{-6} cm^2 s^{-1} (52, 26, 7). If, however, a significant fraction of the indicator is immobilized because of binding to myoplasmic constituents of large molecular weight (e.g., soluble or structural proteins), the apparent diffusion coefficient of the indicator (D_{app}) will be smaller than expected; moreover, the factor by which it is smaller should be related to the ratio of bound indicator molecules to freely diffusible molecules (54).

To estimate D_{app}, resting fluorescence in 5 experiments was measured at different axial distances from the site of fura red injection about an hour (range 48–79 min) after injection. Each data set was fitted by the solution to the one-dimensional diffusion equation (54) to estimate D_{app} and a second parameter (M), proportional to the total quantity of injected indicator. The average value of D_{app} so determined was $0.16\ (\pm 0.01) \times 10^{-6}$ cm^2 s^{-1}. [Note: in 3 of the fibers, D_{app} was estimated from F_{480} measurements alone. In the other 2 fibers, both F_{420} and F_{480} measurements were made, thus allowing two estimates of D_{app} per fiber. In the latter fibers, the average value of D_{app} estimated from the F_{420} and F_{480} data differed by less than 3%; thus the average D_{app} from the 5 fibers is reported.]

Since D_{app} is only ~0.16 of the value expected if all the fura red molecules are freely diffusible, a large fraction of indicator, ~0.84, appears to be bound to relatively immobile myoplasmic constituents. This fraction is larger than the 0.6 value estimated for fura-2 (molecular weight of 637, D_{app} of $0.36\ (\pm 0.03) \times 10^{-6}$ cm^2 s^{-1}; reference 7) but smaller than the 0.9 value estimated for azo-1, another indicator of the tetracarboxylate family (molecular weight of 660, D_{app} of $0.10\ (\pm 0.02) \times 10^{-6}$ cm^2 s^{-1}; ref. 43).

Anisotropy. If fura red is bound to immobile myoplasmic constituents, the rotational mobility, as well as the translational mobility, of the indicator should be reduced. Thus, as was previously found for fura-2 (32), the fluorescence anisotropy of the indicator may be elevated above the value expected for the viscosity of myoplasm, ~2.0 cP. To test this idea, indicator a in myoplasm was estimated by means of Eq. 3 and compared with in vitro values obtained in a 2.0 cP solution without protein. In the latter solution, a was essentially identical for the Ca^{2+}-free and Ca^{2+}-bound forms of the indicator, with the following average values measured at the two excitation wavelengths: $a(420) = 0.259 \pm 0.003$ and $a(480) = 0.280 \pm 0.001$. In contrast, a in resting fibers was significantly higher: $a(420) = 0.335 \pm 0.006$ and $a(480) = 0.348 \pm 0.002$. From the curve in Fig. 6 *D* and the corresponding estimates from Fig. 6 *A* and 6 *C* of the fraction of fura red bound to aldolase, the fiber a values (0.335 and 0.348) imply that 0.54 and 0.70, respectively, of the fura red molecules are associated with proteins of large molecular weight. Thus the measurements of a, like those of D_{app}, indicate that a large fraction of fura red in myoplasm is bound to relatively immobile myoplasmic constituents such as soluble proteins.

Note: as described in Methods, at each of the excitation wavelengths, a was in fact measured with two forms of polarized light, one oriented parallel and the other perpendicular to the fiber axis. The a values did not differ significantly as a function of the polarization of the excitation beam. Thus, there was no indication from the fiber a data that fura red was bound to oriented proteins accessible to myoplasm, such as the myofilaments.

Estimation of f_r, the fraction of fura red in the Ca^{2+}-bound form in resting fibers

To estimate $[Ca^{2+}]_r$, our first step was to estimate f_r. In principal, f_r may be estimated from either fura red's resting absorbance spectrum or its resting fluorescence ratio signal. With either method, the estimate will vary with the choice of the in vitro calibration condition and the associated optical calibration constants. As described in Part I of Results, fluorescence ratio calibrations varied

widely for the in vitro conditions examined (Table 1); in contrast, indicator absorbance spectra (0 and sat. Ca^{2+}) appeared to be less sensitive to the in vitro conditions (Figs. 2 and 4 *A*). This observation is consistent with the general finding that absorbance is less sensitive than fluorescence to the local chemical environment (e.g., reference 44, p. 444). Thus, we have used fura red's myoplasmic absorbance spectrum as our primary means for estimating f_r. As described below, however, a combination of both absorbance and fluorescence measurements permits an evaluation of how f_r may vary with distance from the injection site and with $[D_T]$. These latter variables are important to consider in the estimation of f_r under physiological conditions, since injection damage can artifactually elevate f_r, whereas possible Ca^{2+}-complexation effects associated with a large $[D_T]$ might artifactually lower f_r.

Absorbance. Fig. 7 illustrates the method used to estimate f_r from resting absorbance measurements alone. Panel *A* plots absorbance measured at eleven wavelengths, from a fiber region located a short distance (~200 μm) from the site of fura red injection, where indicator concentration was large (0.5–0.6 mM) and differences in the measurements as a function of wavelength were readily resolved. The 'raw' absorbance levels in panel *A*, which were measured with two forms of linearly polarized light, reflect the fiber's intrinsic absorbance as well as the indicator's absorbance. Panel *B* estimates the indicator-related absorbance, obtained from the data in panel *A* by subtraction of the intrinsic absorbance (estimated by the procedure described in the legend of Fig. 7). Because each absorbance measurement was made at a slightly different time, the data in panel *B* have also had a small correction applied to remove this time dependence (see legend of Fig. 7). Since the indicator-related absorbances were not significantly different as a function of polarization, these data were averaged, with a 1:1 weighting, for further analysis. The averaged data are shown as filled circles in panel *C*, also repeated in panel *D*.

The curves in panel *C* represent in vitro absorbance spectra of fura red in a 2.0 cP salt solution without added protein (cf. Fig. 2 *D*). The dashed curves correspond to 0 and sat. Ca^{2+} conditions (i.e., $f = 0$ and $f = 1$, with curves denoted $A_0(\lambda)$ and $A_{sat}(\lambda)$, respectively). The curves in panel *D* are similar, except that the in vitro measurements are from a solution containing 55 mg/ml aldolase (cf. Fig. 4 *A*). In each panel a least-squares fit determined the scaling constants x and y such that $x*A_0(\lambda) + y*A_{sat}(\lambda)$ gave a best fit to the muscle data (shown as the *continuous curve*). The fraction $y/(x+y)$ estimates f_r, which was 0.14 in panel *C* and 0.32 in panel *D*. Additionally, the fitted value of fura red's absorbance at the isosbestic wavelength can, via Beer's law and the extinction coefficient given in Methods, be used to estimate $[D_T]$ (see legend of Fig. 7).

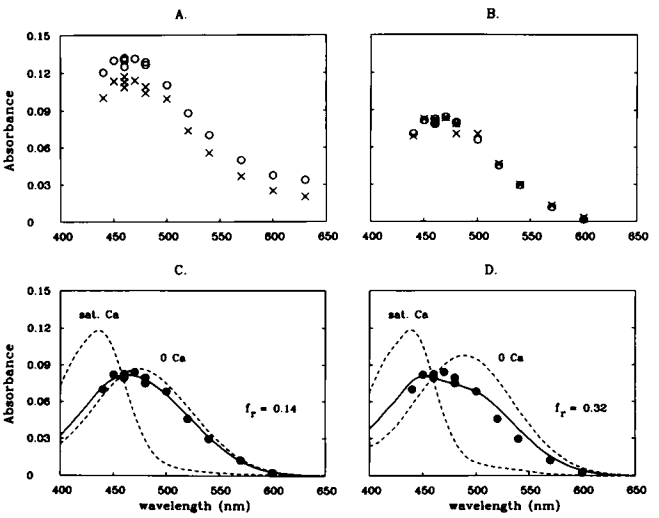

FIGURE 7 Estimation of f_r (the fraction of fura red in the Ca^{2+}-bound form at rest) from a fiber's resting absorbance data. (*A*) Fiber absorbance (intrinsic plus dye-related) measured at eleven wavelengths with 90° (crosses) and 0° (circles) polarized light. (*B*) The indicator-related absorbance, obtained from the data in *A* by subtraction of the fiber intrinsic absorbance; the latter was estimated at each λ by scaling the absorbance at 630 nm (a wavelength where fura red has no absorbance) by the factor $(\lambda/630)^Y$, where $Y = 1.3$ for 90° light and $Y = 1.1$ for 0° light (74). The data in *B* were also corrected, by interpolation, for a small variation in indicator concentration that arose because of diffusion of indicator away from the measurement site. (*C* and *D*) The solid circles show the average (1:1 weighting) of the 90° and 0° data in *B*. The continuous curve in each panel is a least-squares fit of these data by a linear combination of 0 and sat. Ca^{2+} spectra (dashed curves). In *C*, the dashed curves reflect a viscosity of 2.0 cP (without aldolase), the average of the 1.1 and 2.9 cP curves in Fig. 2 *D*. In *D*, the dashed curves were measured at 1.6 cP in the presence of 55 mg/ml aldolase. As described in the text, the scaling constants derived from the least-squares fit determine the estimate of f_r: 0.14 (panel *C*) and 0.32 (panel *D*). From the absorbance at the isosbestic wavelength (458 nm for panel *C*, 459 nm for panel *D*), Beer's law applied with the extinction coefficients given in Methods gives the estimates of $[D_T]$: 0.516 mM (panel *C*) and 0.570 mM (panel *D*). Fiber 091691.2, fiber diameter 113 μm.

The fitting procedures illustrated in panels *C* and *D* of Fig. 7 were carried out in a total of 6 fibers. Column 2 of Table 2 lists the estimates of f_r and column 1 the estimates of $[D_T]$. The value of f_r estimated from the 55 mg/ml aldolase calibration was, on average, 1.9 (±0.1) times that estimated from the 2.0 cP calibration. Column 3 of Table 2 lists the sum-of-squares deviations for the fits, which were substantially larger, on average 3.4 (±0.5) times larger, if based on the aldolase calibration than if based on the 2.0 cP calibration. This finding suggests, but does not prove, that f_r estimated with the 2.0 cP calibration may be more accurate than f_r estimated with the aldolase calibration. This suggestion is somewhat surprising in view of the findings noted above that (*a*) in vitro, at fura red = 0.2 mM and aldolase = 55 mg/ml, nearly all of the fura red molecules were bound to aldolase, and (*b*) in vivo, the great majority of fura red mole-

TABLE 2 **Analysis of fura red signals from fibers at rest**

Fiber	Absorbance			Fluorescence			
	$[D_T]$ (mM) (1)	f_r (2)	SSQ (10^{-3}) (3)	F_{420} (mV) (4)	F_{480} (mV) (5)	R_r (6)	f_r (7)
062791.3				242.8	1599.8	0.152	
2.0 cP	0.613	0.153	0.476				0.074
Aldolase	0.673	0.333	1.18				0.213
091691.2				162.6	1130.6	0.144	
2.0 cP	0.516	0.141	0.065				0.037
Aldolase	0.570	0.318	0.308				0.183
110591.2*				132.8	701.2	0.189	
2.0 cP	0.184	0.293	0.014				0.216
Aldolase	0.202	0.447	0.038				0.338
111591.2				360.5	2078.1	0.173	
2.0 cP	0.769	0.159	0.046				0.159
Aldolase	0.851	0.343	0.240				0.287
041692.1**				67.7	380.0	0.178	
2.0 cP	0.218	0.279	0.043				0.178
Aldolase	0.238	0.439	0.098				0.304
041692.3*				129.6	761.9	0.170	
2.0 cP	0.415	0.198	0.041				0.148
Aldolase	0.455	0.370	0.124				0.277
Mean (N = 3)						0.156	
2.0 cP		0.151					0.090
Aldolase		0.331					0.228

The absorbance (columns 1–3) and fluorescence (columns 4–7) signals are summarized from six fibers at rest. For each measurement, columns 1–3 show values of $[D_T]$, f_r, and the sum-of-squares deviation from the fitting routine (SSQ), respectively, when fitted with in vitro absorbance curves from either a 2.0 cP buffer solution or a 55 mg/ml aldolase buffer solution. The fluorescence signals, columns 4–6, show F_{420}, F_{480}, and R_r, respectively. The estimates of f_r, calibrated from the fluorescence signals alone are shown in column 7 for both the 2.0 cP and the 55 mg/ml aldolase conditions from Table 1 (rows 8 and 11, respectively). All fibers were dissected in normal Ringer and, except for fiber 041692.3, transferred to a "high" Ca^{2+} (11.8 mM) Ringer for injection of fura red and all subsequent measurements. Fiber 041692.3 was in high Ca^{2+} Ringer for a 10 min period only (just after the injection of indicator), the measurements being made in normal Ringer. [Note; (*) denotes fibers for which there was some damage at the calibration region (cf. Fig. 13); and (**) denotes a fiber for which measurements were made at the calibration region only and thus there was no indication of the amount of damage due to the injection.] Averages shown at the bottom reflect values from the 3 fibers without asterisks.

cules appeared to be bound to sites of large molecular weight.

Two other experimental findings also raise doubts about the accuracy of the f_r estimates based on the aldolase calibration. Firstly, in the fits of fura red's absorbance change measured in response to an action potential ($\Delta A(\lambda)$; fits described in detail in connection with Fig. 9 *A* below), the sum-of-squares deviation was again substantially larger for fits based on the aldolase calibration than those based on the 2.0 cP calibration. Secondly, in one experiment at an unusually large fura red concentration (~2.95 mM), $\Delta A(\lambda)$ had a clearly detected *blue-shift* of ~5 nm. This experiment therefore directly supports the conclusion that the myoplasm contains sites that, unlike aldolase, blue-shift the indicator's spectrum. Thus we suppose that the experimental finding that the muscle spectra (both resting and active) are better fitted with the 2.0 cP calibration spectra than with the aldolase spectra represents a somewhat fortuitous situation that arises because fura red is in fact bound to at least two types of sites—those that (like aldolase) induce a red-shift in the indicator's spectrum and those that (like the sites identified in Fig. 9 *B*) induce a blue-shift.

Estimation of f_r based on a mixture of red- and blue-shifted absorbance spectra. If fura red's spectrum in myoplasm exists in both red- and blue-shifted states, one wonders how the simultaneous presence of these states affects the accuracy of f_r estimated with the 2.0 cP absorbance calibration (which, as mentioned above, may be more accurate than f_r estimated with the aldolase calibration). In order to get some information on this point, fits of the muscle $A(\lambda)$ data were carried out under the assumption that half of the fura red molecules in myoplasm are bound to sites that induce a 10-nm red shift in the indicator's spectra (both Ca^{2+}-free and Ca^{2+}-bound) whereas the other half are bound to sites that induce a 10-nm blue shift in the spectra. Additionally, a 10% reduction in spectral amplitude was assumed for the Ca^{2+}-bound forms of the indicator (whether red- or blue-shifted), similar to the finding noted in Fig. 4 *A* in the presence of aldolase.

For these fits, absorbance calibration spectra ($A_0(\lambda)$ and $A_{sat}(\lambda)$), with properties as assumed for each of the two hypothetical binding sites, were constructed from the 2.0 cP spectra, which were taken as (unshifted) standards. The hypothetical red- and blue-shifted spectra

were then combined with a 1:1 weighting and the composite $A_0(\lambda)$ and $A_{sat}(\lambda)$ were used to re-fit the absorbance data from the experiments of Table 2. For each fiber, the fitted value of f_r was slightly larger (on average, 20% larger) than the estimate listed in column 2 of Table 2 for the 2.0 cP absorbance calibration. In each fit, the sum-of-squares deviation was also slightly larger (on average, 22% larger) than that observed in the 2.0 cP fit. Based on this result, we conclude that the fits with the 2.0 cP absorbance calibration, although lacking a firm theoretical justification, provide a reasonable method of estimation of f_r from the muscle $A(\lambda)$ data. It will be considered below which of the fibers in Table 2 are likely to have $[Ca^{2+}]_r$ levels unaltered by injection damage and the presence of indicator.

Fluorescence. f_r may also be estimated from the indicator's fluorescence ratio signal in a resting fiber (denoted R_r). In particular, rows 8 and 11 of Table 1 give fluorescence calibration constants corresponding to the 2.0 cP condition and the 55 mg/ml aldolase condition, respectively. (See Fig. 3 for an example of how a set of in vitro fluorescence constants yield a calibration curve to convert R values to f values.) Columns 4–6 of Table 2 give the values of F_{420}, F_{480}, and R_r measured in the 6 experiments. For the fiber region analyzed in Fig. 7, R_r was 0.144 (the average of the values 0.142 and 0.146, which were measured just before and just after the absorbance measurements shown in Fig. 7). The corresponding estimate of f_r obtained from the 2.0 cP R calibration curve was 0.037, whereas that obtained from the 55 mg/ml aldolase calibration curve was considerably larger, 0.183 (column 7 of Table 2; fiber 091691.2). Similar, although less dramatic, differences in the fluorescence estimates of f_r were seen for the other fibers of Table 2. On average ($N = 6$), the value of f_r estimated from the aldolase fluorescence calibration was 2.7 (±0.6) times that estimated from the 2.0 cP fluorescence calibration. Because, as mentioned above, fluorescence calibration constants varied strongly with the choice of in vitro conditions, and because our fluorescence measurements have no redundancy to provide sum-of-squares information, it is difficult to evaluate the relative accuracy of f_r estimated with the two fluorescence calibrations used in Table 2.

Fura red signals in response to an action potential

Important additional information about the Ca^{2+}-indicator properties of fura red in myoplasm comes from measurements of absorbance and fluorescence changes in response to electrical stimulation of the fiber. The traces in Fig. 8 are examples of changes measured in response to a single action potential initiated at zero time. On the upper left, original transmission changes are shown at 5 wavelengths (indicated in nm to the left). The trace at 630 nm, a wavelength where fura red has no absorbance, reflects a small transmission change intrinsic to the fiber; at the other wavelengths, a large fura red-related change is present in addition to the small intrinsic change. The 630 nm record was used to estimate and remove the intrinsic change at the other wavelengths (cf. legend of Fig. 8); the 4 traces on the upper right of the figure, calibrated in absorbance units, estimate the indicator-related signal. The wavelength dependence of this signal is qualitatively that expected for a change in concentration of Ca^{2+}-fura red complex (Δ[CaD]; cf. Fig. 4C).

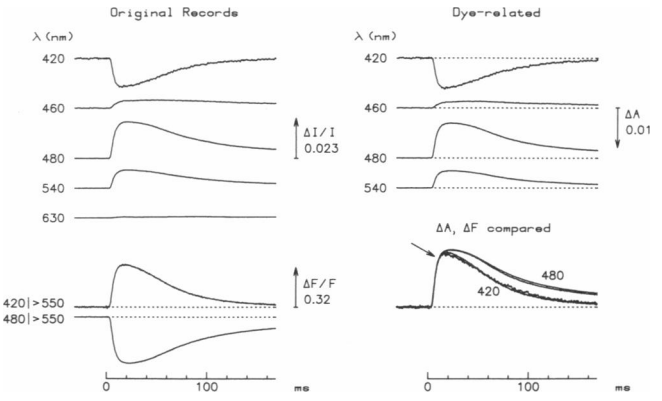

FIGURE 8 Fura red absorbance and fluorescence signals in response to an action potential initiated at zero time. On the left, the top five records show the average of the changes in transmitted intensity for 90° and 0° polarized light at the wavelengths indicated to the left. The bottom two records show changes in fluorescence intensity (emission $\lambda > 550$ nm) for two excitation wavelengths (420 and 480 nm, as indicated), measured at the same time and from the same fiber region as the transmission changes. The four records on the upper right are the dye-related transmission changes (calibrated in ΔA units), obtained from the corresponding records on the left by subtraction of the fiber intrinsic change, estimated from the 630 nm record scaled by the factor $(\lambda/630)^{1.6}$ (75). At the bottom right, the time course of ΔF and ΔA records have been compared after inversion of the 480 nm fluorescence and 420 nm transmission records. All records were scaled so that the rising phases of the signals (up to the time indicated by the arrow) are identical. The divergence in the waveforms at later times is thought to reflect a movement artifact. Y_2, the correction factor calculated from Eq. 5, was for the resting state, 1.154 at 420 nm excitation and 1.142 at 480 nm excitation, and, at 10 ms after stimulation, 1.163 at 420 nm excitation and 1.134 at 480 nm excitation. Fiber 110591.2; see Tables 2 and 3 for additional information about these measurements.

Note: the ΔA traces in Fig. 8 represent the average of ΔA traces recorded with two forms of linearly polarized light (0° and 90°, see Methods). As was found with the measurements of resting absorbance and resting anisotropy, the ΔA measurements were essentially identical with the two forms of polarized light. Thus, the ΔA measurements also gave no indication that fura red is bound to oriented structures within the fiber.

The two traces at the lower left of Fig. 8 show fluorescence changes (with the excitation and emission wavelengths indicated to the left) measured from the same region of the fiber and at the same time as the transmission measurements. Large changes of opposite polarity are seen, as expected for an underlying Δ[CaD]. How-

ever, the falling phases of these ΔF signals do not have an identical time course, a finding not expected if ΔF reflects only Δ[CaD]. Thus, one or both of the ΔF signals reflects at least one other kinetic component. The additional component is related to the presence of fura red, since ΔF signals measured at the same gain from fiber regions not containing fura red were flat (not shown).

The lower right hand side of Fig. 8 compares the time courses of the ΔA and ΔF changes measured with 420 and 480 nm incident light. Apart from a scaling factor, these 4 waveforms are identical during a large fraction of their rising phases. By the times of their peaks, however, and throughout the falling phases, the 420 and 480 nm waveforms are different. Interestingly, the ΔA and ΔF signals obtained with the same incident wavelength have essentially identical waveforms. Since the time at which the 420 and 480 nm traces begin to differ is close to the usual time of onset of fiber mechanical activity (which was not recorded in this experiment), it is possible that a movement artifact accounts for most or all of the additional kinetic component in these signals. Moreover, in other experiments (e.g., fiber 091691.2, not shown), the 420 and 480 waveforms differed at later times in a manner opposite to that shown in Fig. 8, i.e., the 480 waveforms returned to baseline more rapidly than the 420 waveforms. Fiber-to-fiber variability of this type supports the idea that a movement artifact is the source of the extra kinetic component. In the fiber of Fig. 8, the polarity of the extra component is qualitatively consistent with there being a slight decrease in the fiber's optical path length at the time of the mechanical activity. This could arise if the central region of the fiber (where the optical measurements were made) rotated slightly or was stretched and thinned due to fiber shortening at the tendon ends (where sarcomere overlap and tension development are expected to be significant, even in a highly stretched fiber; 55). Fig. 11, described in detail below, illustrates use of the individual ΔF_{420} and ΔF_{480} signals to calculate the fluorescence ratio signal during activity, a signal which should be insensitive to artifacts related to changes in path length or $[D_T]$ (cf. 3).

Spectral dependence of ΔA. In Fig. 9 *A*, the *X*'s plot the normalized spectral dependence of the ΔA signal from the experiment of Fig. 8 (for the wavelengths shown in Fig. 8 plus several additional wavelengths). Each curve in Fig. 9 *A* represents a least-squares fit of a Ca^{2+} difference spectrum for a particular in vitro calibration condition (*continuous curve,* for the 2.0 cP condition; *dashed curve,* for the aldolase condition). The muscle data are clearly better fitted by the curve for the 2.0 cP condition than that for the aldolase condition, a finding that was true not only for this fiber but in general. For the 6 experiments of Table 3, the sum-of-squares deviation for the aldolase fit was, on average, 3.4 (±0.4) times larger than that for the 2.0 cP fit (column 4 of Table 3). This finding suggests, but does not prove, that conclusions from the ΔA data may be more accurate if based on fits with the 2.0 cP curve than the aldolase curve.

From the relative amplitude of the fits in Fig. 9 *A* and the absolute amplitude of the ΔA signals measured in Fig. 8, Δ[CaD] may be calculated from Beer's law and the molar extinction coefficient change given in Methods. The values of Δ[CaD] calculated for the fiber of Figs. 8–9 were 74 μM for the 2.0 cP calibration and 64 μM for the aldolase calibration (cf. column 2 of Table 3). These estimates, in combination with the corresponding estimates of $[D_T]$ from the resting $A(\lambda)$ measurements from this fiber (cf. column 1 of Table 2), allow estimation of $\Delta f (= \Delta[\text{CaD}]/[D_T])$, the change in the fraction of indicator in the Ca^{2+}-bound form during activity. The absolute fraction of indicator in the Ca^{2+}-bound form during activity (denoted f') is then given by $f' = f_r + \Delta f$. Column 3 of Table 3 gives the estimated value of f' for the 6 experiments of Table 2. Column 1 of Table 3 gives the time after stimulation at which each f' value was estimated; this time was selected to just precede the onset of the movement artifact in that experiment. In each of the 6 experiments, this time preceded the time to peak of the 420 waveform, which in turn preceded the time to peak of the 480 waveform (cf. Fig. 8, lower right).

Panel *B* of Fig. 9 shows similar data and fits from another experiment, in which $[D_T]$ at the measurement site was ~2.95 mM. This was the only experiment in which $[D_T]$ at any measurement location exceeded 1 mM. Neither calibration curve in Fig. 9 *B* provides a particularly good fit to the ΔA measurements. For example, the isosbestic wavelength for the muscle data (estimated by linear interpolation to be 453 nm) was clearly less than that for either Ca^{2+}-difference spectrum (458 nm for the 2.0 cP curve and 459 nm for the aldolase curve). At longer wavelengths, 500-600 nm, the muscle data are also clearly blue-shifted in comparison with either curve. The $\Delta A(\lambda)$ signal from this experiment therefore directly supports the hypothesis (mentioned above) that the myoplasm contains binding sites that blue-shift fura red's absorbance spectra. For the 6 fibers of Tables 2 and 3 ($[D_T]$'s in the range 0.2–0.8 mM), the blue-shifting effect of these sites, however, appears to be quite small. For example, if the $\Delta A(\lambda)$ signal from each of these fibers was fitted by the 2.0 cP difference spectrum blue-shifted by variable amounts, the fit with the smallest sum-of-squares deviations was obtained, on average, with a blue shift of 1.2 (±0.2) nm.

[Note: the detection of a blue-shift at larger $[D_T]$ may be rationalized by the idea that the myoplasm contains a saturable number of sites that both blue- and red-shift the indicator's spectra, but that the blue-shifting sites bind the indicator with lower affinity than do the red-shifting sites.]

Fluorescence signals during fiber activity. Columns 5–7 of Table 3 summarize information about fluores-

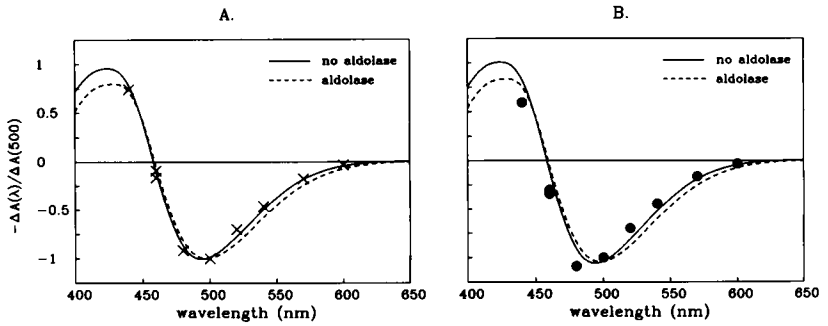

FIGURE 9 The symbols plot the λ-dependence of fura red's absorbance change in response to an action potential, normalized by the change at λ = 500 nm. The relative amplitude at each λ was determined by a least-squares fit of the rising phase of the $\Delta A(\lambda)$ signal with that of the $\Delta A(480)$ signal (up to the time of onset of the movement artifact; see, for example, arrow in Fig. 8, lower right); amplitudes were then normalized to that of $\Delta A(500)$. (*A*) same experiment as Fig. 8 ($[D_T]$ = ~0.2 mM); (*B*) fiber 040792.1, $[D_T]$ = ~2.95 mM fura red. In each fiber, the muscle absorbance spectrum was least-squares fitted with Ca^{2+}-difference spectra reflective of two calibration conditions: 0 mg/ml aldolase, 2.0 cP (continuous curve) and 55 mg/ml aldolase, 1.6 cP (dashed curve). See Tables 2 and 3 for additional information about fiber 110591.2. In the case of fiber 040792.1, the 2.0 cP condition yielded estimates for f, and f' of 0.246 and 0.406, respectively, whereas the aldolase condition yielded estimates of 0.407 and 0.541, respectively; the time after stimulation for the measurement of f' was 6.0 ms. The sum-of-squares deviations based on the aldolase fits were larger (by 5- and 1.5-fold; fits of f, and Δf, respectively) than those based on the 2.0 cP condition.

cence changes recorded at the same time as the ΔA changes of columns 2–4. Columns 5 and 6 give the values of $F_{420} + \Delta F_{420}$ (denoted F'_{420}) and $F_{480} + \Delta F_{480}$ (denoted F'_{480}) measured at the time after stimulation indicated in column 1, whereas column 7 gives the fluorescence ratio signal at this time (denoted R' and calculated as $R' = F'_{420}/F'_{480}$). Column 8 gives the f' value calibrated from the R' value for the 2.0 cP condition and

TABLE 3 Analysis of fura red signals during fiber activity

		Absorbance			Fluorescence			
Fiber	Time (ms) (1)	Δ[CaD] (mM) (2)	f' (3)	SSQ (4)	F'_{420} (mV) (5)	F'_{480} (mV) (6)	R' (7)	f' (8)
062791.3	10.0				305.3	1248.0	0.245	
2.0 cP		0.204	0.486	0.0325				0.375
Aldolase		0.176	0.594	0.1074				0.487
091691.2	6.0				210.5	890.1	0.236	
2.0 cP		0.166	0.462	0.0291				0.353
Aldolase		0.127	0.541	0.0560				0.466
110591.2*	10.0				172.9	484.3	0.357	
2.0 cP		0.074	0.695	0.0234				0.577
Aldolase		0.064	0.765	0.1012				0.695
111591.2	10.0				460.9	1556.2	0.296	
2.0 cP		0.284	0.529	0.0275				0.481
Aldolase		0.246	0.632	0.0757				0.593
041692.1**	12.0				91.3	256.5	0.356	
2.0 cP		0.093	0.705	0.0209				0.576
Aldolase		0.080	0.775	0.1011				0.693
041692.3*	8.0				172.0	562.5	0.306	
2.0 cP		0.166	0.599	0.0256				0.499
Aldolase		0.143	0.685	0.0902				0.612
Mean (N = 3)							0.259	
2.0 cP			0.492					0.403
Aldolase			0.589					0.515

The absorbance (columns 2–4) and fluorescence (columns 5–8) signals are summarized from six fibers during action potential stimulation. Column 1 shows the time after stimulation that the values of both absorbance and fluorescence were determined; this time just preceded onset of a probable movement artifact in the individual records. For each fiber, columns 2–4 show values of Δ[CaD], f' and the sum-of-squares deviation from the fitting routine (SSQ), respectively, when fit with in vitro spectrophotometer difference spectra from either 2.0 cP buffer solutions or 55 mg/ml aldolase buffer solutions. The fluorescence signals, columns 5–7, show F'_{420}, F'_{480}, and R', respectively. Column 8 shows the value of f' if calibrated from the fluorescence signals alone. The asterisks next to the three fiber numbers have the same meaning as in Table 2. Averages shown at the bottom reflect values from the 3 fibers without asterisks.

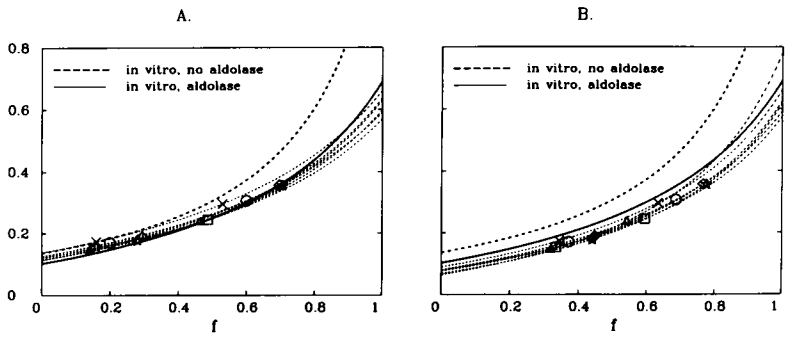

FIGURE 10 "In situ" calibration curves for 6 fibers, obtained from the data in Tables 2 and 3. For each fiber (X's, 111591.2; squares, 062791.3; triangles, 091691.2; circles, 041692.3; stars, 041692.1; diamonds, 110591.2), the fluorescence ratio signals at rest and during activity (R, and R', respectively) were plotted as a function of the corresponding fraction of indicator in the Ca^{2+}-bound form (f, and f', respectively). The f values were determined from fiber absorbance spectra best-fitted with in vitro absorbance spectra for two conditions (panel A: 2.0 cP, no aldolase; panel B: 1.6 cP, 55 mg/ml aldolase). The in situ calibration curve for each fiber (thin dashed curve) was obtained from the ratio of the lines determined by the F_{420} and F_{480} signals measured at rest and during activity (see text). Also shown in each panel are the ratio calibration curves for two in vitro conditions: 2.0 cP, no aldolase (thick dashed curve) and 1.6 cP, 55 mg/ml aldolase (thick solid curve; same as the dashed curve in Fig. 4 D).

for the aldolase condition (calibration constants taken from rows 8 and 11 of Table 1, respectively). The f' value estimated for the aldolase condition was somewhat (on average, ~24%) larger than that estimated for the 2.0 cP condition. An analogous finding was observed in absorbance calibrations, where the estimate of f' for the aldolase condition was, on average, ~16% larger than that for the 2.0 cP condition (cf. column 3 of Table 3).

An in situ calibration of the fluorescence ratio signal

For each of the experiments of Tables 2 and 3, the absorbance and fluorescence data may be combined to construct an "in situ" calibration for the myoplasmic R signal. The in situ curve may be used to calibrate fiber R signals measured in other circumstances, e.g., from fiber regions distant from the injection site where it is not possible to make accurate measurements of $A(\lambda)$.

In Fig. 10, each symbol type represents data from one of the experiments, with R, and R' values (*ordinate*) being plotted as a function of f, and f' values (*abscissa*), respectively; for these plots, the f, and f' values were estimated from absorbance calibrations only (column 2 of Table 2 and column 3 of Table 3, respectively). In panel A, the f estimates from the 2.0 cP absorbance calibration were used, whereas in panel B those from the aldolase absorbance calibration were used. In each panel, the two data points for a particular experiment determine a complete in situ R calibration curve for that fiber (the thin dashed curve intersecting the two data points for that fiber). This curve is uniquely determined since the individual 420 and 480 fluorescence values were measured for two significantly different values of f (at rest and after electrical stimulation [cf. cols 4–5 of Table 2 and cols. 5–6 of Table 3]). Thus, as in the in vitro calibration of Fig. 3, at each wavelength the pair of data points determine a line, and the ratio of the two lines (420 divided by 480) determines the R calibration curve. Methodologically, the in vitro and in situ calibrations are somewhat different, however. For the in vitro calibrations, the f values lie at 0 and 1 and are known; for the in situ calibrations, the f values lie between 0 and 1 and are estimated (from the absorbance fits). The in situ and in vitro calibrations both assume that the fluorescence of fura red arises from 2 states of the indicator: Ca^{2+}-free and Ca^{2+}-bound. If fura red in myoplasm exists in multiple states (e.g., protein-free, protein-bound to sites that red-shift the indicator's absorbance, protein-bound to sites that blue-shift the indicator's absorbance, etc. [each of which can be Ca^{2+}-free and Ca^{2+}-bound]), then the in situ curve should approximate the average behavior of the Ca^{2+}-free and Ca^{2+}-bound states.

In panel A of Fig. 10 the thick dashed curve and the continuous curve correspond to the 2.0 cP condition and the aldolase condition, respectively (calibration constants from rows 8 and 11 of Table 1). These same R curves are also shown in panel B of Fig. 10. It is clear that the R curve from the 2.0 cP condition (*thick dashed curve*) does not agree well with the in situ curves, whether the latter's abscissa data are based on absorbance calibrations in a 2.0 cP solution (panel A) or in the presence of aldolase (panel B). In contrast, the R curve for the aldolase condition (*continuous curve*) is in much better agreement with the in situ calibrations, although the agreement appears somewhat better in panel A than in panel B. Even in panel A, however, systematic discrepancies, both at small and at large values of f, exist between the in situ curves and the continuous curve. Thus, conversion of a fiber's R, signal to f, units may be more accurate if based on the in situ rather than the aldolase calibration curve.

From panel A of Fig. 10, the average values (±SEM) of R_{MIN} and R_{MAX} for the 6 in situ curves were 0.122 (±0.004) and 0.614 (±0.014), respectively; in panel B the average values were 0.076 (±0.004) and 0.642 (±0.031), respectively. For the parameter that deter-

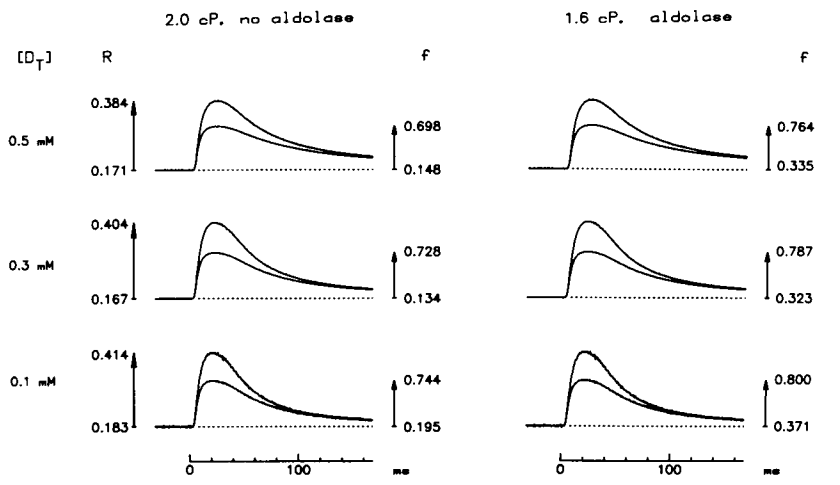

FIGURE 11 Fura red $R(t)$ and $f(t)$ signals recorded from three regions of the same fiber, each of which contained a different concentration of indicator (indicated in mM to the left); zero time marks the moment of action potential stimulation. Within each pair of traces, the larger trace (calibration arrow on the left) is the fluorescence ratio signal ($R(t) = (F_{420} + \Delta F_{420}(t))/(F_{480} + \Delta F_{480}(t))$, whereas the smaller trace (calibration arrow on the right) is $f(t)$, the fractional occupancy of the indicator by Ca^{2+}. The numbers at the lower and upper ends of the arrows show the estimated values of the variables in the resting state and at the peak of activity, respectively. Within each pair of traces, the vertical gain was set to make the traces superimpose for small changes. At each of the indicator concentrations, the $R(t)$ waveform in part A is identical to that in part B. In part A and part B, $f(t)$ was obtained from $R(t)$ by this fiber's in situ calibration curve shown in Fig. 10 A and B, respectively (fiber 111591.2). The recording sites were located 200, 400 and 600 μm from the injection site (upper, middle and lower traces, respectively), where fluorescence signals (F_{420} and F_{480}), but not absorbance signals, were recorded; at 100 μm from the injection site, both absorbance and fluorescence signals (not shown) were recorded, whereby the fluorescence correction factors (Y_2 in Eq. 5) could be calculated for all the locations (see Methods). For any particular location, the estimated concentration of fura red depended on the extinction coefficient used to convert from absorbance units (or indirectly, from fluorescence levels) to indicator concentration. For part A assumed $\epsilon(458) = 21{,}000\ M^{-1}\ cm^{-1}$, appropriate to an in situ calibration of the type shown in Fig. 10 A, $[D_T]$'s of 493, 253 and 84 μM were calculated for the upper, middle, and lower traces, respectively; for part B assumed $\epsilon(459) = 18{,}700\ M^{-1}\ cm^{-1}$, appropriate to an in situ calibration of the type shown in Fig. 10 B, $[D_T]$'s of 545, 281 and 92 μM were calculated. The values of Y_2 for the upper, middle and lower traces, were, respectively: (a) in the resting state, 1.182, 1.160 and 1.145 for 420 nm excitation, and 1.186, 1.156 and 1.134 for 480 nm excitation; (b) at 10 ms after stimulation, 1.200, 1.171 and 1.149 for 420 nm excitation, and 1.169, 1.146 and 1.131 for 480 nm excitation. At other times t after stimulation, the value of $Y_2(t)$ was determined by linear interpolation, based on the measured $\Delta F(t)$ signal and the values of F and Y_2 determined at rest and at 10 ms after stimulation. Fiber diameter, 83 μm; A_f(630 nm), 0.043.

mines the curvature of the R vs. f relationship (namely, the ratio of F_{480} at $f = 0$ to F_{480} at $f = 1$), the values were 0.391 (±0.008) and 0.325 (±0.013) for the in situ calibrations of panels A and B, respectively (F data not shown in Fig. 10). In general, all of these values are less than the analogous values given in Table 1 for the various in vitro calibration conditions, except for the condition with 55 mg/ml aldolase.

A correction for movement artifacts based on the fluorescence ratio signal

Given fiber measurements of F_{420} and F_{480} at rest and of ΔF_{420} and ΔF_{480} during activity, it is straightforward to calculate the fluorescence ratio signal at all times t during activity, $R(t) = (F_{420} + \Delta F_{420}(t))/(F_{480} + \Delta F_{480}(t))$. The $R(t)$ signal is presumably less sensitive than the individual $\Delta F(t)$ signals to possible changes in path length or $[D_T]$, e.g., that may result from fiber mechanical activity (see above). In Fig. 11 A, within each pair of traces the larger trace (calibrated by the arrow on the left) is an example of such an $R(t)$ signal. The three $R(t)$ waveforms shown from this experiment were obtained from fluorescence measurements from three fiber regions, each of which contained a different concentration of fura red (indicated in mM to the left of the traces). After selection of an R calibration curve, each $R(t)$ signal may be converted, on a point-by-point basis, to its corresponding $f(t)$ signal. In Fig. 11 A, the smaller trace of each pair of traces shows the $f(t)$ waveform estimated from the fiber's in situ calibration curve given in Fig. 10 A. The $f(t)$ traces in panel B of Fig. 11 were obtained by a similar procedure except that the fiber's in situ calibration curve in Fig. 10 B was used for the conversion. In both panels of Fig. 11, the $f(t)$ waveforms scale identically with the $R(t)$ waveforms for small changes, but for large changes the $f(t)$ waveforms are proportionally smaller, as expected for R calibration curves that are concave upward. A comparison of panels A and B of Fig. 11 reveals that the resting and peak levels of $f(t)$, but not the shape of $f(t)$, are sensitive to the choice of the calibration curve used to convert $R(t)$ to $f(t)$.

In either panel A or panel B of Fig. 11, a comparison of the three $f(t)$ signals reveals that, as $[D_T]$ increases, the peak amplitude of $f(t)$ decreases and the half-width of $f(t)$ increases. Similar changes in waveform with increasing $[D_T]$ were seen in the case of fluorescence signals recorded in fibers injected with fura-2 (7, 56). These changes are presumed to reflect the increase in the cal-

cium buffering power of myoplasm that is associated with the increase in indicator concentration.

A kinetic estimate of the Ca^{2+}-fura red dissociation constant in myoplasm

In Fig. 11, the lowermost traces show examples of $R(t)$ and $f(t)$ waveforms recorded from a fiber region in which the Ca^{2+}-buffering power of myoplasm should not be increased significantly by the presence of fura red. For the $f(t)$ signal, the time to peak and half-width of the waveform were 20 and 60 ms, respectively. Similar values were observed in a total of 4 experiments, with the average (±SEM) values for the time to peak and half-width being 20 (±2) ms and 62 (±3) ms, respectively (for fiber regions that contained 20-100 μM fura red). These values are similar to those reported for the time to peak and half-width of the $f(t)$ signal from fura-2 at $[D_T] \leq 0.1$ mM, namely, ~20 ms and 50-60 ms, respectively (7). These times, however, are very much slower than those of the underlying myoplasmic free Ca^{2+} transient that drives the $f(t)$ signal. For $\Delta[Ca^{2+}]$, the average values for the time to peak and half-width were 6 ms and 9-10 ms (29, 30) if measured under otherwise identical experimental conditions with a nonbuffering concentration of a rapidly-reacting Ca^{2+} indicator such as purpurate-diacetic acid (28) or furaptra (30). In the case of both fura-2 and fura red, the large discrepancy between the time course of the $\Delta[Ca^{2+}]$ and $f(t)$ signals presumably arises because of delays determined by the effective on- and off-rate constants (denoted k_{+1} and k_{-1}, respectively) of the indicator's reaction with Ca^{2+} in the myoplasmic environment.

As was previously shown for azo-1 (5) and fura-2 (6, 7), a comparison of the amplitude and time course of $\Delta[Ca^{2+}]$ with that of the indicator $f(t)$ permits estimation of k_{+1} and k_{-1} in myoplasm, and hence also of K_D ($=k_{-1}/k_{+1}$). Moreover, in action potential experiments, reasonably accurate estimates of k_{+1} and k_{-1} can be obtained even if the $\Delta[Ca^{2+}]$ and $f(t)$ waveforms are selected from different fibers, as long as the relative time course of the two waveforms is known (S. M. Baylor and S. Hollingworth, unpublished observation from azo-1 and fura-2 experiments). Relative time course information can be determined if, for example, the intrinsic birefringence signals from the two experiments are available as temporal benchmarks to permit relative alignment of the waveforms (cf. 57). The traces in Fig. 12 show examples of $\Delta[Ca^{2+}]$ and $f(t)$ waveforms, which were measured in separate experiments with non-buffering concentrations of furaptra and fura red, respectively. Fig. 12 also shows a best fit of the $f(t)$ trace, obtained under the assumption that $f(t)$ represents a single site response driven by $\Delta[Ca^{2+}]$; for the fit, k_{+1} and k_{-1} were taken as adjustable parameters (cf. legend of Fig. 12). Fits similar to those in Fig. 12 were carried out for four fura red experiments. For each experiment, three separate estimates of k_{+1} and k_{-1} were made, based on fits with $\Delta[Ca^{2+}]$'s measured in three furaptra experiments. Moreover, for each fura red experiment, the kinetic fits were carried out for the $f(t)$ waveforms estimated from both types of in situ calibration curves (Figs. 10–11, parts *A* and *B*, respectively). The average estimates of k_{+1} and k_{-1} were, respectively: for the in situ calibration of Fig. 10 *A*, 1.9 (±0.2) × 10^7 M^{-1} s^{-1} and 19 (±1) s^{-1}; for the in situ calibration of Fig. 10 *B*, 1.9 (±0.2) × 10^7 M^{-1} s^{-1} and 18 (±2) s^{-1}. The estimates of K_D ranged between 0.50 and 1.62 μM for the former calibration and between 0.40 and 1.61 μM for the latter calibration; the average K_D from all of the estimates was 1.05 μM. This value is intermediate between the 0.36 μM and 1.59 μM values determined in the in vitro measurements in the absence and presence of aldolase (Fig. 5). It should be noted that the method of estimation of K_D in Fig. 12 relies on the assumption of a single (and hence spatially-uniform) pool of Ca^{2+} and indicator in the myoplasm. In fact, $\Delta[Ca^{2+}]$ in response to a single action potential is likely to be spatially non-uniform (58); thus, the estimated value of K_D, 1.05 μM, could involve some inaccuracy.

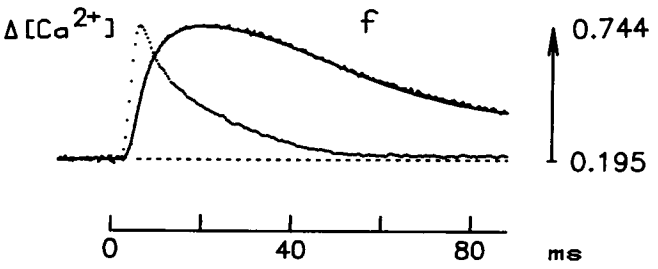

FIGURE 12 Estimation of the effective on- and off-rate constants (denoted k_{+1} and k_{-1}, respectively) of the Ca^{2+}-fura red reaction in myoplasm. Zero-time marks the moment of action-potential stimulation. The trace labelled $\Delta[Ca^{2+}]$ is the waveform of the myoplasmic free Ca^{2+} transient previously recorded in a fiber (052589.2) with furaptra, a rapidly-reacting Ca^{2+} indicator (30). Two traces, labeled f, are shown. The noisier trace is identical to the $f(t)$ measurement shown in the lower-left panel of Fig. 11. The smoother trace is a least-squares fit of the noisier trace, under the assumption that $f(t)$ reflects a single-site reaction driven by $\Delta[Ca^{2+}]$. (The fit is good, making it difficult to distinguish the two traces.) For the fit, the peak amplitude of $\Delta[Ca^{2+}]$ was set to be a 10 μM increase above resting, the average increase inferred from previous action potential experiments (29, 30). The fitted values of k_{+1} and k_{-1} were 1.65 × 10^7 M^{-1} s^{-1} and 24 s^{-1}, respectively. The value of $[Ca^{2+}]_r$ used in the fit, 0.35 μM, is consistent with an f_r of 0.195 and the calculated K_D ($=k_{-1}/k_{+1}$) of 1.45 μM.

Estimation of the resting myoplasmic free $[Ca^{2+}]$ level

After assumption of a particular value of K_D, $[Ca^{2+}]_r$ can be calculated (via Eq. 4) for each experimental estimate of f_r. It is important to consider, however, whether injection damage or $[D_T]$ changes f_r from its normal value. Information on this question is available in Fig. 13, which shows examples from 3 experiments (two on the

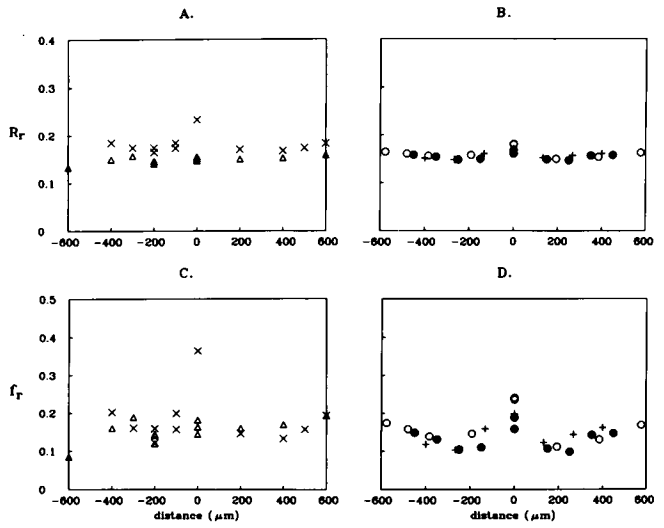

FIGURE 13 The ordinate plots Ca^{2+}-related signals recorded from resting fibers (the ratio signal, parts *A* and *B*; the estimated fraction of fura red in the Ca^{2+}-bound form, parts *C* and *D*) as a function of axial distance from the site of fura red injection (abscissa). In *A* and *C*, each symbol type refers to one experiment: triangles (fiber 091691.2, sarcomere length 3.5 μm), *X*'s (fiber 111591.2, sarcomere length 3.8 μm); the measurements in these fibers were made in 11.8 mM Ca^{2+} Ringer. In *B* and *D*, the data are all from the same fiber (041692.3), which was in 1.8 mM Ca^{2+} Ringer. Each symbol type refers to a particular sarcomere length: 2.5 μm (filled circles; data collected 17–30 min after injection); 3.8 μm (+'s; 38–45 min after injection) and 2.6 μm (open circles; 65–71 min after injection). For the plots in *B* and *D*, the original *x*-axis locations of the 3.8 μM and 2.6 μm data sets were scaled by the factors 2.5/3.8 and 2.5/2.6, respectively, in order that the distance scale would reference the same location on the fiber for all sarcomere lengths. For all fibers, the R_r signal was converted to f_r units by means of that particular fiber's in situ calibration curve from Fig. 10 *A*.

left, one on the right) of R_r values (upper panels) and corresponding f_r values (lower panels) measured at different axial distances from the injection site. For each experiment, the R_r data were converted to f_r values by means of that particular fiber's in situ calibration given in Fig. 10 *A* (2.0 cP condition), which is thought to be more accurate than the in situ calibration of Fig. 10 *B* (55 mg/ml aldolase condition). On the left, the data were all obtained at long sarcomere length: 3.8 μm for fiber 111591.2 (*X*'s) and 3.5 μm for fiber 091691.2 (*triangles*). On the right, all data were obtained from the same fiber (041692.3), but at 3 different sarcomere lengths: 2.5 μm (*closed circles*), 3.8 μm (+'s) and 2.6 μm (*open circles*). For the fiber on the right and for one of the fibers on the left (*X* data), f_r (and therefore $[Ca^{2+}]_r$) values at the injection site are clearly elevated in comparison with the values measured at the other locations; these localized elevations presumably reflect some local damage caused by the injection (cf. 15). In the other fiber on the left (*triangle data*), f_r at the injection site was not elevated in comparison with the other measurements; thus injection damage appeared to be minimal in this experiment. The data from these and other experiments (not shown) suggest that an estimate of $[Ca^{2+}]_r$ not influenced by injection damage can usually be obtained from fluorescence measurements made 200 μm or more from the injection site, where R_r measurements generally show little variation with distance. Moreover, at locations ≥ 300 μm from the injection site, $[D_T]$ is usually sufficiently small (e.g., ≤0.2 mM) that the indicator concentration is not likely to influence $[Ca^{2+}]_r$ because of Ca^{2+} buffering. Thus, if $[Ca^{2+}]_r$ is estimated from such fiber regions, the estimate should be minimally influenced by both injection damage and by $[D_T]$. It should be noted that R_r, in contrast to $A(\lambda)$, can be reliably estimated from fiber regions for which $[D_T] \leq$ 0.2 mM; thus, the fluorescence data from these fiber regions are essential for obtaining estimates of f_r and $[Ca^{2+}]_r$ at small values of $[D_T]$.

Table 4 summarizes estimates of f_r and $[Ca^{2+}]_r$ from fiber regions that contained both large and small $[D_T]$ and that appeared to be minimally affected by injection damage. Column 2 lists average values of f_r estimated under six calibration assumptions (see legend of Table 4), and cols. 3-5 give corresponding estimates of $[Ca^{2+}]_r$ calculated from Eq. 4 with three assumed values of K_D (indicated in μM at the top of the columns). The values of K_D in columns 3 and 5 are those determined under in vitro conditions in the absence and presence of aldolase, respectively (cf. Fig. 5), whereas that in column 4 reflects the average value estimated from the kinetic fits discussed in the preceding section. In part *A* of the table, the measurement regions were located 100–250 μm from the injection site and therefore contained relatively large concentrations of fura red, 0.5–0.8 mM; in parts *B* and *C*, the measurement regions were 200–900 μm from the injection site and thus contained smaller indicator concentrations, 0.02–0.2 mM. The estimates of $[Ca^{2+}]_r$ span a wide range. An asterisk denotes those estimates that we think combine the most reliable calibration methods with the most probable values of K_D in the myoplasmic environment. These estimates, 0.19–0.33 μM, lie outside the range of $[Ca^{2+}]_r$ values measured or commonly assumed for frog skeletal muscle fibers, 0.02–0.12 μM (48, 17, 18, 13, 6, 7, 15).

Do the estimates of $[Ca^{2+}]_r$ depend on $[D_T]$?

Parts *A* and *C* of Table 4 reflect estimates of $[Ca^{2+}]_r$ at higher (0.5–0.8 mM) and lower (0.02–0.2 mM) $[D_T]$, respectively. In other respects the estimates are comparable, since the estimates for part *C* depend directly (via in situ *R* calibration curves) on simultaneous absorbance and fluorescence data measured from the same fiber regions used for the absorbance estimates in part *A* of the table. The estimates of $[Ca^{2+}]_r$ at higher $[D_T]$ are slightly (15%) smaller than those obtained at lower $[D_T]$. The difference in the estimates is in the direction expected if fura red, which was injected into the myoplasm from a

TABLE 4 **Summary of estimates of f_r and $[Ca^{2+}]_r$ from fura red**

Calibration method (1)	f_r (2)	$[Ca^{2+}]_r$ (nM) for the specified values of K_D (μM): K_D = 0.36 (3)	K_D = 1.05 (4)	K_D = 1.59 (5)
A. Absorbance				
2.0 cP	0.151 ± 0.005	64	187*	283*
Aldolase	0.331 ± 0.007	178	520	787
B. Fluorescence				
2.0 cP	0.111 ± 0.025	45	131	199
Aldolase	0.247 ± 0.021	118	344	522
C. In situ				
2.0 cP	0.173 ± 0.014	75	220*	333*
Aldolase	0.350 ± 0.012	194	565	856

Fura red estimates of f_r and $[Ca^{2+}]_r$, obtained with several calibration methods (column 1). Column 2 estimates f_r (mean ± SEM), the fraction of fura red in the Ca^{2+}-bound form at rest. For each mean value of f_r, the remaining columns of the table estimate $[Ca^{2+}]_r$, by means of Eq. 4 in the text, for the indicated value of K_D (the apparent dissociation constant of fura red for Ca^{2+} in the myoplasmic environment). The values of K_D in column 3 and 5 are the estimates from the in vitro solutions that contained no aldolase and 55 mg/ml aldolase, respectively (see Fig. 5), whereas that in column 4 represents the average value estimated by the method illustrated in Fig. 12 (see text). In part *A*, the estimate of f_r in the rows labelled "2.0 cP" and "aldolase" were obtained from fura red's absorbance signal, by the method described in connection with Fig. 7 *C* and Fig. 7 *D*, respectively. Means and SEM's were calculated from column 2 of Table 2 for the three fibers not marked by an asterisk (i.e., the fibers for which the absorbance measurements were minimally affected by the injection process). In part *B*, f_r was estimated from R_r measurements, by means of in vitro calibration curves of the type shown in Fig 3 *B*. The calibration curves were determined by the constants given in rows 8 and 11 of Table 1 (corresponding, respectively, to the rows labelled "2.0 cP" and "aldolase" in part *B* of this table). The mean and SEM calculations are based on 5 of the 6 experiments listed in Table 2; fiber 041692.1 was not included in this analysis because R_r data as a function of distance from the injection site were not recorded in this fiber. For each fiber analyzed, a single R_r value was determined that reflected the average of the measurements from all regions of that fiber that were at least 200 μm from the injection site and that contained 0.02–0.2 mM fura red (2–4 measurements per fiber). In part *C*, f_r values were determined from the same R_r values analyzed in part *B*; however, in each experiment, the curve used to convert R_r to f_r was that fiber's "in situ" calibration curve, shown in either Fig. 10 *A* or Fig. 10 *B* (corresponding, respectively, to the rows labelled "2.0 cP" and "aldolase" in part C of this table). Of the 18 estimates of $[Ca^{2+}]_r$, the entries indicated by an asterisk are considered to reflect the most reliable calibration techniques and the most likely values of K_D.

pipette containing no added Ca^{2+}, binds myoplasmic Ca^{2+} and thus lowers $[Ca^{2+}]_r$. The magnitude of the effect is small, however, for the range of $[D_T]$'s used in the experiments.

Does $[Ca^{2+}]_r$ depend on sarcomere length?

The estimates of $[Ca^{2+}]_r$ in Table 4 were made from highly-stretched fibers, with sarcomere lengths of 3.5–4.0 μm in the region of optical recording. There are several reports in the literature that $[Ca^{2+}]_r$ in frog fibers, measured with both aequorin (59–61) and with Ca^{2+}-selective electrodes (62), may increase at longer sarcomere lengths. Thus it is possible that our $[Ca^{2+}]_r$ estimates in Table 4 are substantially higher than the physiological level due to the long sarcomere length of our fibers.

To investigate this possibility, measurements of the type shown on the right-hand side of Fig. 13 were recorded. In this experiment, R_r values at several fiber locations were measured, first at a shorter sarcomere length (2.5 μm), then at a longer sarcomere length (3.8 μm), and again at a shorter sarcomere length (2.6 μm). For fiber regions located 100 or more μm from the injection site, R_r (Fig. 13 *B*) and therefore f_r (Fig. 13 *D*) values did not decrease with increasing distance from the injection site and thus are not likely to be influenced by injection damage. At these measurement locations, R_r and f_r varied little with sarcomere length. Minimal effects of sarcomere length were also seen in 2 other experiments (fibers 040792.2 and 081192.1). These fibers, like the fiber of Fig. 13, *B* and *D*, were exposed to high Ca^{2+} Ringer for a short period (5–20 min) at the time of, or immediately after, the injection of indicator in order to aid fiber recovery from any injection damage; then the fibers were returned to normal Ringer for bracketed measurements of R_r at shorter (2.5–2.9 μm) and longer (3.5–3.8 μm) sarcomere lengths. For the three fibers, f_r, estimated at regions located 100–500 μm from the injection site by in situ calibration curves of the type shown in Fig. 10 *A*, was increased only slightly with stretch [from 0.133 (±0.013) at short sarcomere length to 0.141 (±0.011) at long sarcomere length]. This change was not statistically significant. A small, also nonsignificant, increase in f_r, from 0.168 (±0.024) at short sarcomere length to 0.191 (±0.018) at long sarcomere length, was observed at the injection site, where both sarcomere length and injection damage likely influence the result. For the regions away from the injection site, the increase in the mean value of f_r with stretch, if real, corresponds to an increase in $[Ca^{2+}]_r$ of 7% (independent of the choice of K_D). Thus, in our experiments, a change in sarcomere length in the range 2.5–3.8 μm appears to have at most a minor effect on $[Ca^{2+}]_r$. A possible expanation for the striking effect of sarcomere length reported in reference 62 is that Ca^{2+}-electrode measurements, which necessar-

ily report $[Ca^{2+}]_r$ at the impalement site, reflect a variable component due to injection damage and that this component increases substantially with stretch.

Does the $[Ca^{2+}]$ level of Ringer affect $[Ca^{2+}]_r$?

The measurements described in the preceding section were carried out on fibers bathed in normal Ringer ($[Ca^{2+}] = 1.8$ mM). However, most of the experiments of this article were carried out on fibers that, although dissected in normal Ringer, were transferred to high-Ca^{2+} (11.8 mM) Ringer for the duration of the experiment (the exception being fiber 041692.3 [see legend of Table 2]). The question thus arises whether the relatively large values of $[Ca^{2+}]_r$ estimated in Table 4 (numbers denoted by an asterisk) might be a consequence of the elevated level of $[Ca^{2+}]$ in the Ringer.

Preliminary information on this question is available from a comparison of the data in Table 4 with the data from the fibers in normal Ringer, discussed in the preceding section. For the latter fibers, the average value of f_r at long sarcomere length was 0.141, whereas the estimate of f_r in Table 4, obtained by a comparable calibration technique, was 0.173 (row 5, column 2). This suggests that high-Ca^{2+} Ringer may be associated with an elevation in $[Ca^{2+}]_r$ of ~25%.

More direct information on this question was obtained in two experiments. Fiber 040692.1 was in high-Ca^{2+} Ringer for a period of 35 min, during which time the fiber was injected with fura red and initial fluorescence and absorbance measurements were made. At the end of this period, the value of R_r was measured 150 μm from the injection site (sarcomere length = 3.8 μm) and found to be 0.175. The bath solution was then changed to normal Ringer and R_r was remeasured at the same location 1 and 5 min later; the recorded values, 0.175 and 0.174, were indistinguishable from the value measured in high-Ca^{2+} Ringer. Thus the Ringer Ca^{2+} concentration appeared to have no effect on $[Ca^{2+}]_r$ in this fiber.

In the second fiber (040792.2; sarcomere length also 3.8 μm), the effect of Ringer $[Ca^{2+}]$ was studied at a location 300 μm from the injection site. The first measurement of R_r, taken after the fiber had been in 11.8 mM $[Ca^{2+}]$ for 19 min, was 0.159. The bath solution was then changed to normal Ringer; R_r, measured 1 and 47 min later, was 0.149 and 0.144, respectively. Finally, Ringer $[Ca^{2+}]$ was changed back to 11.8 mM; the value of R_r, measured 3 min later, was 0.144. Thus, the average values of R_r observed in 11.8 mM and 1.8 mM Ca^{2+} Ringer were 0.1515 and 0.1465, respectively. These values, if calibrated by the average of the in situ calibration curves shown in Fig. 10 *A*, correspond to f_r levels of 0.140 and 0.118, respectively. From Eq. 4, $[Ca^{2+}]_r$ appeared to be ~22% higher in 11.8 mM than in 1.8 mM $[Ca^{2+}]$ Ringer (independent of K_D). Thus, the 25% increase in $[Ca^{2+}]_r$ estimated from the two populations of fibers appears to be in reasonable agreement with the 0–22% increases estimated for the two experiments described here.

DISCUSSION

This article describes absorbance and fluorescence signals from fura red, both in vitro and in frog single muscle fibers. A comparison of the in vitro and in vivo signals has permitted: (*a*) a characterization of a number of properties of fura red in the myoplasmic environment; (*b*) an estimation of f_r, the fraction of the indicator in the Ca^{2+}-bound form in a resting fiber; and (*c*) an estimation of $[Ca^{2+}]_r$, the resting level of myoplasmic free $[Ca^{2+}]$. To our knowledge, our experiments with fura red represent the first direct use, in any cell, of absorbance measurements from an indicator to estimate $[Ca^{2+}]_r$. Because absorbance measurements are less sensitive to the local chemical environment than are fluorescence measurements (cf. 44), estimation of $[Ca^{2+}]_r$ may be more reliable with absorbance measurements than with fluorescence measurements.

Analogous estimates of $[Ca^{2+}]_r$ in frog fibers might, in principle, be made with other high-affinity indicators, such as fura-2 or quin-2, that undergo a large absorbance change with Ca^{2+} complexation. The principal absorbance bands of these indicators, however, are at ultraviolet wavelengths, where interference from the intrinsic absorbance of the fiber is substantially greater than at the visible wavelengths used with fura red (cf. 34, 35). Thus, at similar myoplasmic concentrations of indicator, estimation of the indicator-related absorbance is expected to be more accurate with fura red than with fura-2 or quin-2. Unfortunately, other tetracarboxylate Ca^{2+} indicators with absorbance bands at visible wavelengths are unsuited for estimation of $[Ca^{2+}]_r$ by the methods described in this article, either because their affinity for Ca^{2+} is too low (e.g., azo-1, with a K_D for Ca^{2+} of ~4 μM) or because the absorbance change of the indicator with Ca^{2+} complexation is minimal (e.g., fluo-3 or calcium green). Thus, of currently-available Ca^{2+} indicators, fura red is uniquely suited in muscle fiber experiments for (*a*) estimation of $[Ca^{2+}]_r$ by means of absorbance measurements and (*b*) construction of "in situ" calibration curves of the type shown in Fig. 10 to permit interpretation of the fluorescence ratio signal.

Alteration of the properties of fura red by the myoplasmic environment

As described in the in vitro measurements (Part I of Results), aldolase, an abundant intracellular protein, had, at 55 mg/ml, a major effect on the indicator's fluorescence signal and some effect on the indicator's absorbance signal. Aldolase also increased, by ~4-fold, the indicator's K_D for Ca^{2+}. Thus, estimates of intracellular $[Ca^{2+}]$ with fura red depend strongly on the choice of optical signal as well as the particular solution condition used to calibrate the optical signal.

The evidence in Part II of Results indicates that, intracellularly, a large percentage, perhaps as much as 85%, of fura red molecules are bound to myoplasmic constituents of large molecular weight. Moreover, in myoplasm the indicator's K_D as well as its fluorescence calibration constants (R_{MIN}, R_{MAX} and the curvature of the R vs. f relationship) do indeed appear to be altered in comparison with in vitro calibrations in solutions lacking muscle constituents. Surprisingly, little evidence was detected that the absorbance spectra of the indicator, at least at fura red concentrations less than 1 mM, was detectably different in myoplasm compared with a 2.0 cP calibration solution. As discussed in Results, this might represent a somewhat fortuitous net effect, as the constituents found in the myoplasm of frog fibers may, in the case of some constituents, bind and induce a red-shift of the indicator's spectra and, in other cases, bind and induce a blue-shift.

An additional concern, detected in the in vitro calibrations, was an effect of light itself on fura red's fluorescence. This effect appears to be due primarily to a photo-isomerization, not a bleaching, of the indicator. Although the alteration of fura red's fluorescence signals by photo-isomerization represents a potentially serious problem for the intracellular estimation of $[Ca^{2+}]_r$, two findings suggest that in fact this is not a major concern in our experiments. Firstly, in the in vitro calibrations, illumination had little effect on the indicator's absorbance spectra and no detectable effect on K_D; as discussed in Results, our primary estimation of f_r relied on absorbance measurements. Secondly, no effect of illumination on the fluorescence of fura red was detected in muscle fibers. This latter observation is probably related to the findings that, in vitro, protein-bound fura red was much less affected by illumination than protein-free fura red (cf. Part I of Results) and, in vivo, fura red appeared to be heavily bound to muscle constituents of large molecular weight.

Estimation of f_r

We have chosen fura red's intracellular absorbance signal, rather than the indicator's fluorescence ratio signal, as the primary means to estimate f_r. However, as described in Part II of Results, if both absorbance and fluorescence measurements from the same fiber region are available for two fiber states with substantially different $[Ca^{2+}]$ levels (e.g., at rest and as a result of electrical stimulation), it is possible to combine the measurements of A, F, ΔA and ΔF to yield an in situ calibration curve that permits conversion of R to f for any value of R (cf. Fig. 10). The in situ curve has the advantage that it can be used to calibrate R signals from fiber regions removed from the injection site, where effects of injection damage and of indicator concentration on $[Ca^{2+}]_r$ are likely to be small, but where the indicator's resting absorbance signal is too small to be measured reliably. This combination of both absorbance and fluorescence measurements appears to be very useful in the case of our large frog fibers (diameter, $\sim$100 μm), in which $A(\lambda)$, at fura red concentrations $\geq$ 0.2–0.3 mM, can be reliably measured above the background of the fiber's intrinsic absorbance. Unfortunately, an analogous use of fura red's absorbance signal in cells of smaller diameter will probably be difficult to carry out.

Estimation of $[Ca^{2+}]_r$

Column 2 of Table 4 illustrates that conversion of fura red's optical signal to f_r varies with the calibration method (absorbance or fluorescence; with or without proteins; etc.). For the six methods analyzed, the average estimates of f_r varied by a factor slightly greater than 3. After correction for the nonlinearity between f and $[Ca^{2+}]$ (eqn. 4), this variation corresponds to about a 4-fold variation in $[Ca^{2+}]_r$ (for any particular value of K_D). Moreover, the estimates of K_D given in cols. 3–5 of Table 4 vary by a factor slightly greater than 4; thus, overall the estimates of $[Ca^{2+}]_r$ in Table 4 span a nearly 20-fold range. As mentioned in Results, the asterisks in Table 4 denote the estimates of $[Ca^{2+}]_r$ that we think combine the most reliable methods for estimation of f_r with the most probable values of K_D in the myoplasmic environment. The values of these $[Ca^{2+}]_r$ estimates, 0.19–0.33 μM, are substantially larger than the 0.02–0.12 μM range measured and/or commonly assumed for frog fibers (cf. Introduction and Results). It is thus important to consider possible reasons for the elevated estimates of $[Ca^{2+}]_r$ in Table 4.

As discussed in Results, the values of $[Ca^{2+}]_r$ in Table 4 may be elevated by $\sim$7% because of the long sarcomere length ($\geq$3.5 μm) of our fibers and by $\sim$15% because of the use of high Ca^{2+} (11.8 mM) in the Ringer. On the other hand, the lowest of the likely estimates in Table 4 (187 μM) may underestimate the normal value of $[Ca^{2+}]_r$ by $\sim$15% because of the Ca^{2+} buffer capacity of the larger indicator concentrations used for the measurements in part A of the Table (0.5–0.8 mM). Thus, referred to physiogical conditions (low indicator concentration, shorter sarcomere length, 1.8 mM $[Ca^{2+}]$ in Ringer), our range of likely estimates for $[Ca^{2+}]_r$ becomes 0.18 to 0.27 μM.

Although not reported in Results, f_r and $[Ca^{2+}]_r$ are also affected slightly by the levels of pH and Mg^{2+} assumed in the calibrations. In row 1 of Table 4, the average estimate of f_r (0.151) would be reduced by $\sim$3% if the resting $A(\lambda)$ data from the muscle fibers had been analyzed with $A_0(\lambda)$ and $A_{sat}(\lambda)$ spectra appropriate for a free $[Mg^{2+}]$ level of 1 mM, rather than the 0 mM level assumed. Uncertainty about myoplasmic pH in the physiological range has a slightly larger effect on the estimates. For example, the estimate of f_r in row 1 of Table 4 would be elevated (lowered) by about 10% if internal pH were 6.8 (7.2), rather than the assumed value of 7.0. The combined uncertainties due to both pH and Mg^{2+} are

too small, however, to substantially lower our estimates of $[Ca^{2+}]_r$. Our conclusion, therefore, is that $[Ca^{2+}]_r$ in frog fibers is likely to be larger than previously supposed, ~0.2–0.3 μM.

Relationship of $[Ca^{2+}]_r$ to physiological activation of the fiber

$[Ca^{2+}]_r$ in a normal fiber at rest is expected to be below a level that causes significant activation of the myofilaments or the Ca^{2+} pump of the sarcoplasmic reticulum (SR). In measurements with skinned fibers, Ca^{2+}-activated tension usually increases steeply with $[Ca^{2+}]$. For example, at 15–22°C the force-$[Ca^{2+}]$ relationship in frog fibers has a Hill coefficient of 2.8–3.8 and a K_D for half activation of 1.3–1.6 μM (63). These data imply that, even at $[Ca^{2+}]_r$ = 0.3 μM, myofilament activation would be <2% of maximum, consistent with expectations for a resting fiber.

In SR vesicles from frog muscle, studies of the Ca^{2+} pump at $[Mg^{2+}]$ = 1 mM and pH = 7 indicated that, in vesicles not loaded with Ca^{2+}, the pump ATPase rate at $[Ca^{2+}]$ = 0.3 μM is about 20–25% of the maximal Ca^{2+}-stimulated rate (64,65). However, as the SR becomes loaded with Ca^{2+}, the ATPase rate decreases substantially. At $[Ca^{2+}]$ = 0.3 μM, the SR loads to about one-third of the maximum level (64), the approximate load under physiological conditions (66), and the final ATPase rate is estimated to be about one-fifth of the unloaded rate (reference 65, and unpublished observations of Drs. N. Kurebayashi and Y. Ogawa). Thus, in a resting fiber with a normally loaded SR, activation of the Ca^{2+} pump at $[Ca^{2+}]_r$ = 0.3 μM should be small, perhaps ~5% of maximum.

A final question concerns the Ca^{2+}/Mg^{2+} sites on parvalbumin and the role that these sites may play in promoting muscle relaxation (67, 68). For these sites to be effective in capturing Ca^{2+} during the falling phase of the tension response, it is necessary that they be occupied by Mg^{2+} prior to the activation of contraction by Ca^{2+} (for model calculations, see references 69, 48). Thus it is expected that a substantial fraction of the sites (which, in fibers of *Rana temporaria*, are found at large concentration, 1.5–2.0 mM (70)) should be occupied by Mg^{2+} and not Ca^{2+} in the resting state. The resting occupancy of the sites can be calculated from the dissociation constants of the sites and from assumed values of the resting free concentrations of Mg^{2+} and Ca^{2+}. Unfortunately, the dissociation constants for *Rana temporaria* are not available, and the values reported for carp muscle (71, 72) and bullfrog muscle (73) differ by more than an order of magnitude. Thus, more work, preferably with species specific parvalbumins, appears to be required to decide whether a $[Ca^{2+}]_r$ of 0.2–0.3 μM in skeletal fibers from *Rana temporaria* is consistent with the postulated role of parvalbumin in relaxation.

Have other techniques underestimated $[Ca^{2+}]_r$ in intact amphibian muscle fibers?

There have been no definitive estimates of f_r or $[Ca^{2+}]_r$ in intact amphibian fibers injected with fura-2. Suda and Kurihara (10) reported that R_{MIN} in fibers from *Rana temporaria* was lower in myoplasm than in a 0 Ca^{2+}, 0.1 M KCl calibration solution (see also 6), but a quantitative estimate of $[Ca^{2+}]_r$ from the fluorescence ratio signal was not attempted. Lee et al. (9) considered estimates of $[Ca^{2+}]_r$ in toad fibers from fura-2's ratio signal to be unreliable because of uncertainty about whether the intracellular environment significantly reduced R_{MIN} below the in vitro value. (R_{MAX} was certainly reduced, probably by a factor of about 2.8). Baylor and Hollingworth (7) injected fura-2 and antipyrylazo III simultaneously into frog fibers and, by an indirect technique, which involved knowledge of the relative values of the diffusion constants of the two indicators in the myoplasm, estimated f_r; the values fell in the range −0.14 to +0.31 (N = 11). However, because of the indirect nature of the technique, they considered the reliability of these estimates to be uncertain.

Blatter and Blinks (15) made simultaneous estimates of $[Ca^{2+}]_r$ in intact single fibers of *Rana temporaria* with two techniques, aequorin and Ca^{2+}-selective micro-electrodes. The experimental protocols were carefully controlled, both techniques were calibrated with common in vitro solutions, the fibers that had detectable elevations in $[Ca^{2+}]_r$ due to impalement damage were excluded from the analysis, and, in the case of aequorin, allowance was made for a partially identified myoplasmic constituent that altered the calibration of $[Ca^{2+}]$. The average estimates were 38 nM with aequorin and 59 nM with Ca^{2+} micro-electrodes. These estimates represent an upper limit for $[Ca^{2+}]_r$ since a Ringer potassium concentration of 12.5 mM was used in the experiments to elevate $[Ca^{2+}]_r$ to a level where reproducible measurements with aequorin could be made. [Note: in a 1.8 mM $[Ca^{2+}]$ Ringer, an elevation of Ringer potassium from 2.5 to 12.5 mM probably raises $[Ca^{2+}]_r$ by 3-6 fold (unpublished observations of A. B. Harkins, N. Kurebayashi and S. M. Baylor obtained with fluo-3; manuscript in preparation)].

At the present time we cannot reconcile our range of estimates of $[Ca^{2+}]_r$ from fura red, 0.18–0.27 μM, with the results of Blatter and Blinks (15). One possibility is that, for unknown reasons, there was a true difference in $[Ca^{2+}]_r$ in the two sets of experiments. To test this possibility, it would be necessary to make simultaneous measurements of $[Ca^{2+}]_r$ with fura red and one of the other techniques. Another possibility (the explanation that we favor) is that unrecognized calibration difficulties remain to be elucidated, not only for Ca^{2+} indicator dyes, but also for the other techniques used to measure $[Ca^{2+}]_r$.

Has $[Ca^{2+}]_r$ in other cells been underestimated with ratiometric indicators?

Intracellular fluorescence ratio signals (e.g., those from fura-2 and indo-1) are commonly calibrated by fluorescence constants measured in a 0.1 M KCl solution without added protein or sucrose. In the case of fura red, this method would correspond to the use of calibration constants of the type given in the rows of Table 1 marked with an asterisk. If the 5 fibers that contributed to parts *B* and *C* of Table 4 (for which the indicator concentration was $\leq$0.2 mM) had been calibrated by this method, the average value estimated for f_r would have been 0.073, a value less than half of that which we consider likely (0.173, row 5 of Table 4). Moreover, calibration of $[Ca^{2+}]_r$ often assumes that the indicator's K_D is unchanged by the intracellular environment. In the case of frog skeletal muscle fibers, the K_D's of both fura-2 and fura red may be increased as much as 3–4 fold over the values measured in in vitro calibrations without added protein (references 7, 32, 53 and this article). It therefore seems possible that ratiometric calibrations as commonly applied to other cell types may have underestimated $[Ca^{2+}]_r$ substantially.

We thank Dr. Y. Ogawa and Mr. Murayama of the Juntendo University School of Medicine for a gift of a supernatant fraction from bullfrog muscle, and Drs. S. Hollingworth and M. Konishi for comments on the manuscript.

This work was supported by the National Institues of Health, grants NS-17620 (to S.M.B.) and 2-T32-HL-07027 (pre-doctoral training grant to A.B.H.), and by a travel grant from the Sankyo Foundation of Life Sciences (to N.K.).

Received for publication 26 October 1992 and in final form 4 January 1993.

REFERENCES

1. Tsien, R. Y. 1980. New calcium indicators and buffers with high selectivity against magnesium and protons: design, synthesis, and properties of prototype structures. *Biochemistry.* 19:2396–2404.
2. Tsien, R. Y., T. Pozzan, and T. J. Rink. 1982. Calcium homeostasis in intact lymphocytes: Cytoplasmic free calcium monitored with a new, intracellularly trapped fluorescent indicator. *J. Cell Biol.* 94:325–334.
3. Grynkiewicz, G., M. Poenie, and R. Y. Tsien. 1985. A new generation of Ca^{2+} indicators with greatly improved fluorescence properties. *J. Biol. Chem.* 260:3440–3450.
4. Minta, A., J. P. Y. Kao, and R. Y. Tsien. 1989. Fluorescent indicators for cytosolic calcium based on rhodamine and fluorescein chromophores. *J. Biol. Chem.* 264:8171–8178.
5. Baylor, S. M., S. Hollingworth, C. S. Hui, and M. E. Quinta-Ferreira. 1985. Calcium transients from intact frog skeletal muscle fibres simultaneously injected with antipyrylazo III and azo 1. *J. Physiol.* 365:70P.
6. Klein, M. G., B. J. Simon, G. Szucs, and M. F. Schneider. 1988. Simultaneous recording of calcium transients in skeletal muscle using high- and low-affinity calcium indicators. *Biophys. J.* 53:971–988.
7. Baylor, S. M., and S. Hollingworth. 1988. Fura-2 calcium transients in frog skeletal muscle fibres. *J. Physiol.* 403:151–192.
8. Westerblad, H., J. A. Lee, A. G. Lamb, S. R. Bolsover, and D. G. Allen. 1990. Spatial gradients of intracellular calcium in skeletal muscle during fatigue. *Pflugers Archiv.* 415:734–740.
9. Lee, J. A., H. Westerblad, and D. G. Allen. 1991. Changes in tetanic and resting $[Ca^{2+}]_i$ during fatigue and recovery of single muscle fibres from Xenopus Laevis. *J. Physiol.* 433:307–326.
10. Suda, N., and S. Kurihara. 1991. Intracellular calcium signals measured with fura-2 and aequorin in frog skeletal muscle fibers. *Jap. J. Physiol.* 41:277–295.
11. Rudel, R., and S. R. Taylor. 1973. Aequorin luminescence during contraction of amphibian skeletal muscle. *J. Physiol.* 233:5P–6P.
12. Blinks, J. R., R. Rudel, and S. R. Taylor. 1978. Calcium transients in isolated amphibian skeletal muscle fibres: detection with aequorin. *J. Physiol.* 277:291–323.
13. Cannell, M. B. 1986. Effect of tetanus duration on the free calcium during the relaxation of frog skeletal muscle fibres. *J. Physiol.* 376:203–218.
14. Konishi, M., and S. Kurihara. 1987. Effects of caffeine on intracellular calcium concentration in frog skeletal muscle fibres. *J. Physiol.* 383:269–283.
15. Blatter, L. A., and J. R. Blinks. 1991. Simultaneous measurement of Ca^{2+} in muscle with Ca electrodes and aequorin. Diffusible cytoplasmic constituent reduces Ca^{2+}-independent luminescence of aequorin. *J. Gen. Physiol.* 98:1141–1160.
16. Tsien, R. Y., and T. J. Rink. 1980. Neutral carrier ion-selective micro-electrodes for measurement of intracellular free calcium. *Biochim. Biophys. Acta.* 599:623–638.
17. Lopez, J. R., L. Alamo, C. Caputo, R. DiPolo, and J. Vergara. 1983. Determination of ionic calcium in frog skeletal muscle fibers. *Biophys. J.* 43:1–4.
18. Weingart, R., and P. Hess. 1984. Free calcium in sheep cardiac tissue and frog skeletal muscle measured with Ca^{2+}-selective microelectrodes. *Pflugers Archiv.* 402:1–9.
19. Miledi, R., I. Parker, and G. Schalow. 1977. Measurement of calcium transients in frog muscle by the use of arsenazo III. *Proc. R. Soc. Lond. B.* 198:201–210.
20. Miledi, R., I. Parker, and P. H. Zhu. 1983. Calcium transients in frog skeletal muscle fibres following conditioning stimuli. *J. Physiol.* 339:223–242.
21. Baylor, S. M., W. K. Chandler, and M. W. Marshall. 1979. Arsenazo III signals in singly-dissected frog twitch fibres. *J. Physiol.* 287:23–24P.
22. Baylor, S. M., W. K. Chandler, and M. W. Marshall. 1982. Use of metallochromic dyes to measure changes in myoplasmic calcium during activity in frog skeletal muscle fibres. *J. Physiol.* 331:139–177.
23. Palade, P., and J. Vergara. 1982. Arsenazo III and antipyrylazo III calcium transients in single skeletal muscle fibers. *J. Gen. Physiol.* 79:679–707.
24. Kovacs, L., E. Rios, and M. F. Schneider. 1979. Calcium transients and intramembrane charge movement in skeletal muscle fibres. *Nature (Lond.).* 279:391–396.
25. Kovacs, L., E. Rios, and M. F. Schneider. 1983. Measurement and modification of free calcium transients in frog skeletal muscle fibres by a metallochromic indicator dye. *J. Physiol.* 343:161–196.
26. Maylie, J., M. Irving, N. L. Sizto, and W. K. Chandler. 1987. Calcium signals recorded from cut frog twitch fibers containing antipyrylazo III. *J. Gen. Physiol.* 89:83–143.

27. Maylie, J., M. Irving, N. L. Sizto, G. Boyarsky and W. K. Chandler. 1987. Calcium signals recorded from cut frog twitch fibers containing tetramethylmurexide. *J. Gen. Physiol.* 89:145–176.

28. Hirota, A., W. K. Chandler, P. L. Southwick, and A. S. Waggoner. 1989. Calcium signals recorded from two new purpurate indicators inside frog cut twitch fibers. *J. Gen. Physiol.* 94:597–631.

29. Konishi, M., and S. M. Baylor. 1991. Myoplasmic calcium transients monitored with purpurate indicator dyes injected into intact frog skeletal muscle fibers. *J. Gen. Physiol.* 97:245–270.

30. Konishi, M., S. Hollingworth, A. B. Harkins, and S. M. Baylor. 1991. Myoplasmic calcium transients in intact frog skeletal muscle fibers monitored with the fluorescent indicator furaptra. *J. Gen. Physiol.* 97:271–301.

31. Raju, B., E. Murphy, L. A. Levy, R. D. Hall, and R. E. London. 1990. A fluorescent indicator for measuring cytosolic free magnesium. *Am. J. Physiol.* 256:C540–C548.

32. Konishi, M., A. Olson, S. Hollingworth, and S. M. Baylor. 1988. Myoplasmic binding of fura-2 investigated by steady-state fluorescence and absorbance measurements. *Biophys. J.* 54:1089–1104.

33. DeMarinis, R. M., H. E. Katerinopoulos, and K. A. Muirhead. 1990. New tetracarboxylate compounds as fluorescent intracellular calcium indicators. *Biochem. Meth.* 112:381.

34. Irving, M., J. Maylie, N. L. Sizto and W. K. Chandler. 1987. Intrinsic optical and passive electrical properties of cut frog twitch fibers. *J. Gen. Physiol.* 89:1–40.

35. Konishi, M., N. Suda and S. Kurihara. 1993. Fluorescence signals from the Mg^{2+}/Ca^{2+} indicator furaptra in frog skeletal muscle fibers. *Biophys. J.* 64:223–239.

36. Kurebayashi, N., A. B. Harkins, and S. M. Baylor. 1992. Comparison of characteristics of fura red in vitro with those in single skeletal muscle fibers. *Folia Pharmacologica Japonica.* 100:26P.

37. Kurebayashi, N., A. B. Harkins, and S. M. Baylor. 1992. Use of fura red as a myoplasmic Ca^{2+} indicator in intact frog skeletal muscle fibers. *Biophys. J.* 61:A160.

38. Harafuji, H., and Y. Ogawa. 1980. Re-examination of the apparent binding constant of ethylene glycol bis(β-aminoethyl ether)-N,N,N′,N′-tetraacetic acid with calcium around neutral pH. *J. Biochem.* 87:1305–1312.

39. Martell, A. E., and R. M. Smith. 1974. Critical Stability Constants. Vol. 1: Amino Acids. Plenum Publishing Corp., New York.

40. Poenie, M. 1990. Alteration of intracellular fura-2 fluorescence by viscosity: a simple correction. *Cell Calcium.* 11:85–91.

41. Ottaway, J. H., and J. Mowbray. 1977. Compartmentation in control of glycolysis. *In* Current Topics in Cellular Regulation. Vol 12. B. L. Horecker and E. R. Stadtman, editors. Academic Press, Inc., New York. 107–208.

42. Baylor, S. M., and H. Oetliker. 1977. A large birefringence signal preceding contraction in single twitch fibres of the frog. *J. Physiol.* 264:141–162.

43. Baylor, S. M., S. Hollingworth, C. S. Hui, and M. E. Quinta-Ferreira. 1986. Properties of the metallochromic dyes arsenazo III, antipyrylazo III and azo 1 in frog skeletal muscle fibres at rest. *J. Physiol.* 377:89–141.

44. Cantor, C. R., and P. R. Schimmel. 1980. Biophysical Chemistry. Part II. W. H. Freeman and Co., San Francisco. 439–444.

45. Baylor, S. M., W. K. Chandler, and M. W. Marshall. 1981. Studies in skeletal muscle using optical probes of membrane potential. *In* The Regulation of Muscle Contraction: Excitation-Contraction Coupling. A. D. Grinnell and M. A. B. Brazier, editors. Academic Press, Inc. New York. 97–130.

46. Harrison, S. M., and D. M. Bers. 1987. The effect of temperature and ionic strength on the apparent Ca-affinity of EGTA and the analogous Ca-chelators BAPTA and dibromo-BAPTA. *Biochim. Biophys. Acta.* 925:133–143.

47. Kurebayashi, N., T. Kodama and Y. Ogawa. 1980. P^1, P^5-di(adenosine-5′)pentaphosphate (Ap_5A) as an inhibitor of adenylate kinase in studies of fragmented sarcoplasmic reticulum from bullfrog skeletal muscle. *J. Biochemistry.* 88:871–876.

48. Baylor, S. M., W. K. Chandler, and M. W. Marshall. 1983. Sarcoplasmic reticulum calcium release in frog skeletal muscle fibres estimated from arsenazo III calcium transients. *J. Physiol.* 344:625–666.

49. DeMello, W. C. 1973. Membrane sealing in frog skeletal muscle fibers. *Proc. Natl. Acad. Sci. USA.* 70:982–984.

50. Baylor, S. M., and H. Oetliker. 1975. Birefringence experiments on isolated skeletal muscle fibres suggest a possible signal from the sarcoplasmic reticulum. *Nature (Lond.).* 253:97–101.

51. Becker, P. L., and F. S. Fay. 1987. Photobleaching of fura-2 and its effect on determination of calcium concentrations. *Am. J. Physiol.* 253:C613–C618.

52. Kushmerick, M. J., and R. J. Podolsky. 1969. Ionic mobility in muscle cells. *Science (Wash. DC).* 166:1297–1298.

53. Uto, A., H. Arai, and Y. Ogawa. 1991. Reassessment of fura-2 and the ratio method for determination of intracellular Ca^{2+} concentrations. *Cell Calcium.* 12:29–37.

54. Crank, J. 1956. The Mathematics of Diffusion. Oxford University Press, London.

55. Huxley, A. F., and L. D. Peachey. 1961. The maximum length for contraction in vertebrate striated muscle. *J. Physiol.* 156:150–165.

56. Hollingworth, S., A. B. Harkins, N. Kurebayashi, M. Konishi, and S. M. Baylor. 1992. Excitation-contraction coupling in intact frog skeletal muscle fibers injected with mmolar concentrations of fura-2. *Biophys. J.* 63:224–234.

57. Baylor, S. M., W. K. Chandler, and M. W. Marshall. 1984. Calcium release and sarcoplasmic reticulum membrane potential in frog skeletal muscle fibres. *J. Physiol.* 348:209–238.

58. Cannell, M. B., and D. G. Allen. 1984. Model of calcium movements during activation in the sarcomere of frog skeletal muscle. *Biophys. J.* 45:913–925.

59. Snowdowne, K. W., and N. K. M. Lee. 1980. Subcontracture concentrations of potassium and stretch cause an increase in the activity of intracellular calcium in the frog skeletal muscle. *Fed. Proc.* 39:1733.

60. Snowdowne, K. W. 1986. The effect of stretch on sarcoplasmic free calcium of frog skeletal muscle at rest. *Biochim. Biophys. Acta.* 862:441–444.

61. Hannon, J. D. and L. A. Blatter. 1990. Elevation of $[Ca^{++}]_i$ unmasks stretch-induced increase in resting $[Ca^{++}]_i$ in aequorin-injected frog skeletal muscle fibers. *Biophys. J.* 57:175*a*. (*Abstr.*)

62. Lopez, J. R., L. Alamo & C. Caputo. 1985. The increase in metabolic rate associated with stretching in skeletal muscle might be related to an increment in free $[Ca^{2+}]$. *Biophys. J.* 47:378*a*. (*Abstr.*)

63. Godt, R. E. and B. D. Lindley. 1982. Influence of temperature upon contractile activation and isometric force production in mechanically skinned muscle fibers of the frog. *J. Gen. Physiol.* 80:279–297.

64. Ogawa, Y., N. Kurebayashi, A. Irimajiri & T. Hanai. 1981. Transient kinetics for Ca uptake by fragmented sarcoplasmic reticulum from bullfrog skeletal muscle with reference to the rate of relaxation of living muscle. *In* Adv. Physiol. Sci, Vol. 5, Molecular and Cellular Aspects of Muscle Contraction Excitation-Contraction Coupling. E. Varga, A. Kover, T. Kovacs, and L. Kovacs, editors. Akademiai Kiado Budapest: Pergamon Press. 416–435.

65. Ogawa, Y. and N. Kurebayashi. 1982. ATP-ADP exchange reaction by fragmented sarcoplasmic reticulum from bullfrog skeletal muscle. *J. Muscle Res. Cell Motility.* 3:39–56.

66. Endo, M. 1977. Calcium release from the sarcoplasmic reticulum. *Physiol. Rev.* 57:71–108.

67. Briggs, N. 1975. Identification of the soluble relaxing factor as a parvalbumin. *Fed. Proc.* 34:540.

68. Gerday, C., and J. M. Gillis. 1976. The possible role of parvalbumin in the control of contraction. *J. Physiol.* 258:97–97P.

69. Gillis, J. M., D. Thomason, J. Lefevre, and R. H. Kretsinger. 1982. Parvalbumins and muscle relaxation: A computer simulation study. *J. Muscle Res. Cell Motility.* 3:377–398.

70. Hou, T.-T., J. D. Johnson, and J. A. Rall. 1991. Parvalbumin content and Ca^{2+} and Mg^{2+} dissociation rates correlated with changes in relaxation rate of frog muscle fibres. *J. Physiol.* 441:285–304.

71. Potter, J. D., J. D. Johnson, J. R. Dedman, W. E. Schreiber, F. Mandel, R. L. Jackson, and A. R. Means. 1977. Calcium-binding proteins: Relationship of binding, structure, conformation and biological function. *In* Calcium-binding Proteins and Calcium Function. R. H. Wasserman, R. A. Corradino, E. Carofoli, R. H. Kretsinger, D. H. MacLennan, and F. L. Siegel, editors. Amsterdam: North-Holland. 239–250.

72. Johnson, J. D., D. E. Robinson, S. P. Robertson, A. Schwartz, and J. D. Potter. 1981. Ca^{2+} exchange with troponin and the regulation of muscle contraction. *In* Regulation of Muscle Contraction: Excitation-Contraction Coupling. A. D. Grinnell, and Mary A. B. Brazier, editors. Academic Press, New York. 241–259.

73. Ogawa, Y. and M. Tanokura. 1986. Kinetic studies of calcium binding to parvalbumins from bullfrog skeletal muscle. *J. Biochem.* 99:81–89.

74. Baylor, S. M., and S. Hollingworth. 1990. Absorbance signals from resting frog skeletal muscle fibers injected with the pH indicator dye, phenol red. *J. Gen. Physiol.* 96:449–471.

75. Hollingworth, S., and S. M. Baylor. 1990. Changes in phenol red absorbance in response to electrical stimulation of frog skeletal muscle fibers. *J. Gen. Physiol.* 96:473–491.